Accepted Manuscript

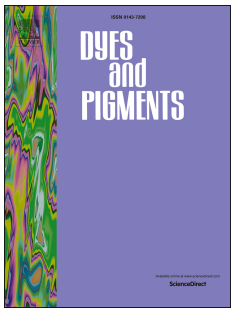

Dicyanoboron Diketonate Dyes: Synthesis, Photophysical Properties and Bioimaging

Yan Zhou, Yu-Zhe Chen, Jian-Hua Cao, Qing-Zheng Yang, Li-Zhu Wu, Chen-Ho Tung, Da-Yong Wu

PII: S0143-7208(14)00278-2

DOI: 10.1016/j.dyepig.2014.07.001

Reference: DYPI 4444

To appear in: *Dyes and Pigments*

Received Date: 26 May 2014

Revised Date: 30 June 2014

Accepted Date: 2 July 2014

Please cite this article as: Zhou Y, Chen Y-Z, Cao J-H, Yang Q-Z, Wu L-Z, Tung C-H, Wu D-Y, Dicyanoboron Diketonate Dyes: Synthesis, Photophysical Properties and Bioimaging, *Dyes and Pigments* (2014), doi: 10.1016/j.dyepig.2014.07.001.

Graphical abstract

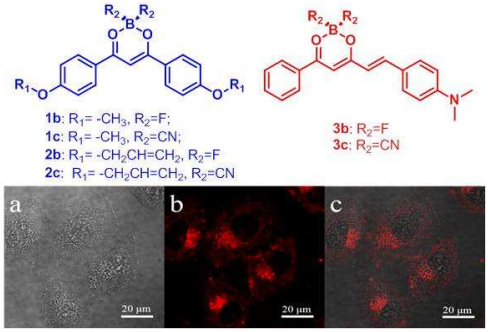

We report a new class of dicyanoboron diketonates complexes which exhibit high molar absorption coefficients, large Stokes shifts, high photostability and low cytotoxicity.

Dicyanoboron Diketonate Dyes: Synthesis, Photophysical Properties and Bioimaging

Yan Zhou[a,b], Yu-Zhe Chen*[a] , Jian-Hua Cao[a], Qing-Zheng Yang[a], Li-Zhu Wu[a], Chen-Ho Tung[a], Da-Yong Wu*[a]

[a] Technical Institute of Physics and Chemistry, Chinese Academy of Sciences, 29 Zhongguancun East Road, Beijing, 100190, China.

[b] University of The Chinese Academy of Sciences, Beijing, 100049, China

* Corresponding author. Fax: +86 10 62554670, Tel: +86 10 82543772.

E-mail: chenyuzhe@mail.ipc.ac.cn (Y. Chen), dayongwu@mail.ipc.ac.cn (D. Wu).

Abstract

A new class of dicyanoboron diketonates ($B(CN)_2$) was synthesized and the photophysical properties were investigated. The $B(CN)_2$ complexes exhibited high molar absorption coefficients, large Stokes shifts, high photostability and low cytotoxicity. Especially, the emission of the $B(CN)_2$ extended into the deep red region. The extensive π conjugation and the presence of intramolecular charge transfer (ICT) transitions are responsible for their red-shifted emission. Their fluorescence are very sensitive to the polarity of the solvents. They are highly emissive in low polarity solvents, but weakly fluorescent in polar solvents. Cell imaging experiments demonstrated its potential application as a probe in bioorganisms due to its excellent imaging contrast. This strategy represents a facile approach to modulate the photophysical properties of dyes.

Keywords

Dicyanoboron diketonate, fluorescence dye, optical properties, solvent effect

1. Introduction

Organoboron complexes are one of the most important types of fluorescent dyes [1]. Notably, because of their large molar extinction coefficients, high emission quantum yields, and sensitivity to the surrounding medium, boron dipyrromethene dyes (BODIPYs) and boron diketonates have attracted much interest in the fields of molecular probes [2,3], optical imaging [4,5], sensing applications [6], and laser dyes [7,8]. In addition to the rich photophysical properties which they share in common with BODIPYs, boron diketonates also show large two photon absorption cross sections, air stability, pronounced room temperature phosphorescence and delayed fluorescence when incorporated with polymer matrices in the solid state [9,10]. Within this context, the synthesis and studies of boron diketonates have gained much attention recently [11]. Various efforts have been made to tune the photophysical properties of the organoboron complexes, which is in essence, the alteration of the transition energy levels of the dye molecules [12]. This change is often effected by chemically modifying the π conjugation or the substituent groups. Extending the absorption and emission properties of the dyes to the deep red/near-infrared region would facilitate their application in biological systems by avoiding interferences from background autofluorescence, minimizing photodamage to samples, and increasing tissue penetration [13]. For organoboron complexes, replacing fluorine with other functional groups such as aryl, ethynylaryl etc. represents a very simple and effective

method for such a purpose. For example, Ziessel et al. have reported on the substitution of fluorine of BODIPY by alkynyl, alkynylaryl, ethynylaryl and aryl groups [14]. Such derivatives share not only improvement of their stabilities but also large Stokes shifts in their emission spectra. In contrast, very few difluoroboron diketonate derivatives, with fluorine replaced by other groups as analogous derivatives, have been reported [15]. Information such as emission properties in solution and the solid state have not yet been studied.

In line with our ongoing work on BODIPY and boron diketonates as fluorescent sensors for the detection of biological thiols and various metal ions in solution and in living cells [16], we decided to extend our investigation toward tuning the photophysical properties of diketonate derivatives. In particular, we intended to design boron 1, 3-diketonate dyes which are fluorescent in the deep red/near-infrared region by simple methods and to apply them for *in vivo* studies. In this paper, we present the synthesis, absorption and fluorescence emission properties, and theoretical calculations of dicyanoboron diketonates ($B(CN)_2$, **1c**-**3c,** Scheme 1). The substitution of fluorine by cyano group red shifted the emission > 25 nm. Especially, the emission of **3c** extended into the deep red region. The $B(CN)_2$ complexes exhibited high molar absorption coefficients, large Stokes shifts, good imaging contrast, high photostability and low cytotoxicity.

Scheme 1. Structures of the difluoroboron diketonates **1b**-**3b** and dicyanoboron diketonates **1c**-**3c**.

2. Experimental Section

2.1 General Experimental Methods

^{1}H and ^{13}C NMR spectra were recorded on an Advance Bruker 400M spectrometer (400 MHz) using tetramethylsilane (TMS) as an internal standard in $CDCl_3$ at room temperature. Mass spectra (ESI) were obtained on Bruker Apex IV Fourier Transform Mass Spectrometer. Mass spectra (EI) were obtained in the positive ion mode on a Waters GCT premier. Fourier-Transform Infrared (FT-IR) Spectra were recorded on a Varian Excalibur 3100 infrared spectrometer. Fluorescence spectra were determined on a Hitachi F-4600 spectrophotometer. Absorption spectra were determined on a Hitachi U-3900 UV-Visible spectrophotometer. Fluorescence lifetimes were recorded on Edinburgh F900 spectrometer. Tetrahydrofuran (THF) was refluxed with sodium in the presence of benzophenone as indicator for 5 h and then distilled under nitrogen. Other reagents were analytical grade and were used without further purification.

2.2 Synthesis

2.2.1 Synthesis of **1a**

1a was synthesized by a standard Claisen condensation under basic conditions according to the literature [17] (Scheme S1). The crude product was recrystallized in ethanol to give **1a** as yellow needle crystals (2.06 g, 72.5%). ^{1}H NMR (400 MHz, $CDCl_3$) δ 17.11 (s, 1H, enol-OH), 7.96 (d, 4H), 7.00 (d, 4H), 6.74 (s, 1H, COCHCO), 3.90 (s, 6H, OCH_3). ^{13}C NMR (100 MHz, $CDCl_3$) δ 192.90, 184.74, 164.09, 163.18, 131.43, 129.70, 129.21, 128.30, 114.09, 91.60, 55.62, 55.57. MS (EI) m/z calcd for $C_{17}H_{16}O_4$ $[M]^+$ 284.10, found 284.11.

2.2.2 Synthesis of **1b**

To a solution of **1a** (1.42 g, 5 mmol) in CH_2Cl_2 (40 mL), boron trifluoride diethyl etherate (1.25 mL, 10 mmol) and triethylamine (1 mL, 7.5 mmol) was added. After being stirred for 6 h at room temperature in the dark, the reaction solution was washed with water (50 mL) and brine (50 mL). The organic layer was dried over anhydrous $MgSO_4$ and the solvent was removed *in vacuo* to give the crude product. Purification by flash column chromatography (silica gel, petroleum/CH_2Cl_2 1:1) gave **1b** as a yellow green powder (1.56 g, 94%) [17]. ^{1}H NMR (400 MHz, $CDCl_3$) δ 8.14 (d, J = 9.0 Hz, 4H), 7.11 – 6.93 (m, 5H), 3.94 (s, 6H, OCH_3). ^{13}C NMR (100 MHz, $CDCl_3$) δ 180.84, 165.32, 131.25, 124.56, 114.57, 91.53, 55.75. MS (EI) m/z calcd for $C_{17}H_{15}O_4BF_2$ $[M]^+$ 332.10, found 332.11.

2.2.3 Synthesis of **1c**

To a solution of **1b** (100 mg, 0.3 mmol) in CH_2Cl_2 (20 mL), trimethylsilyl cyanide (120 μL, 1 mmol) and boron trifluoride diethyl etherate (125 μL, 1 mmol) were added. After stirring at room temperature for 1 h, the reaction solution was washed with water (30 mL) and brine (30 mL). The organic layer was dried over anhydrous $MgSO_4$ and the solvent was removed *in vacuo* to give the crude product. Purification by flash column chromatography (silica gel, petroleum/CH_2Cl_2 1:3) gave **1c** as a yellow powder (55 mg, 53%). ^{1}H NMR (400 MHz, $CDCl_3$) δ 8.12 (d, J = 9.0 Hz, 4H), 7.14 – 6.94 (m, 5H), 3.96 (s, 6H). ^{13}C NMR (100 MHz, $CDCl_3$) δ 179.78, 166.66, 132.08, 123.21, 115.06, 93.65, 55.99. HRMS (ESI) m/z calcd for $C_{19}H_{15}BN_2NaO_4$ $[M+Na]^+$ 369.10205, found 369.10210.

2.2.4 Synthesis of **2a**

2a was synthesized by a standard Claisen condensation as described for **1a** [17] (Scheme S1). Purification by flash column chromatography (silica gel, petroleum/ethyl acetate 4:1) gave **2a** as a dark yellow solid. Yield 70%. ^{1}H NMR (400 MHz, $CDCl_3$) δ 17.09 (s, 1H, enol-OH), 7.94 (d, *J* = 8.9 Hz, 4H), 6.98 (d, *J* = 8.9 Hz, 4H), 6.72 (s, 1H, COCHCO), 6.06 (ddd, *J* = 22.5, 10.6, 5.3 Hz, 2H), 5.44 (d, *J* = 17.3 Hz, 2H), 5.33 (d, *J* = 10.5 Hz, 2H), 4.61 (d, *J* = 5.3 Hz, 4H, OCH_2). ^{13}C NMR (100 MHz, $CDCl_3$) δ 192.55, 184.57, 162.97, 162.07, 132.68, 132.47, 131.27, 129.79, 129.04, 128.44, 118.11, 117.99, 114.71, 114.63, 91.54, 68.93. MS (EI) m/z calcd for $C_{21}H_{20}O_4$ 336.14, found 336.14.

2.2.5 Synthesis of **2b**

2b was synthesized by the same method as **1b**. Purification by flash column chromatography (silica gel, petroleum/CH_2Cl_2 1:2) gave **2b** as a bright yellow powder [17]. Yield 90%. ^{1}H NMR (400 MHz, $CDCl_3$) δ 8.10 (d, *J* = 8.9 Hz, 4H), 7.11 – 6.91 (m, 5H), 6.06 (ddd, *J* = 22.4, 10.5, 5.3 Hz, 2H), 5.45 (d, *J* = 17.3, 2H), 5.35 (d, *J* = 10.5, 2H), 4.65 (d, *J* = 5.2 Hz, 4H, OCH_2). ^{13}C NMR (100 MHz, $CDCl_3$) δ 184.64, 180.94, 164.40, 162.14, 132.74, 132.18, 131.34, 131.23, 129.10, 128.50, 124.77, 118.50, 118.07, 115.31, 114.78, 91.65, 69.23, 69.00. MS (EI) m/z calcd for $C_{21}H_{19}O_4BF_2$ $[M]^+$ 384.13, found 384.14.

2.2.6 Synthesis of **2c**

2c was synthesized by the same method as **1c**. Purification by flash column chromatography (silica gel, petroleum/CH_2Cl_2 1:2) gave **2c** as a yellow solid. Yield

48%. ^{1}H NMR (400 MHz, $CDCl_3$) δ 8.09 (d, *J* = 8.8 Hz, 4H), 7.18 – 6.90 (m, 5H), 6.06 (ddd, *J* = 22.2, 10.4, 5.2 Hz, 2H), 5.46 (d, *J* = 17.3 Hz, 2H), 5.37 (d, *J* = 10.5 Hz, 2H), 4.69 (d, *J* = 4.9 Hz, 4H, OCH_2). ^{13}C NMR (100 MHz, $CDCl_3$) δ 179.71, 165.66, 132.07, 131.72, 129.07, 123.23, 118.91, 118.17, 115.70, 114.69, 93.70, 69.43, 68.94. HRMS (ESI) m/z calcd for $C_{23}H_{19}BN_2NaO_4$ $[M+Na]^+$ 421.13342, found 421.13403.

2.2.7 Synthesis of **3a**

3a was obtained as a white powder by reaction of benzoylacetone and trifluoroboron diethyl etherate. Yield 92%. ^{1}H NMR (400 MHz, $CDCl_3$) δ 8.07 (d, *J* = 7.3 Hz, 2H), 7.70 (t, *J* = 7.5 Hz, 1H), 7.54 (t, *J* = 7.9 Hz, 2H), 6.60 (s, 1H), 2.43 (s, 3H, CH_3). ^{13}C NMR (100 MHz, $CDCl_3$) δ 192.69, 182.91, 135.47, 131.21, 129.21, 129.01, 97.51, 24.75. MS (EI) m/z calcd for $C_{10}H_9O_2BF_2$ $[M]^+$ 210.07, found 210.07.

2.2.8 Synthesis of **3b**

To a solution of **3a** (1.05 g, 5 mmol) in EtOH (60 mL), was added dimethylaminobenzaldehyde (0.89 g, 6 mmol). After it had dissolved completely, hexahydropyridine (60 μL, 6 mmol) was added into the solution. After refluxing at 80℃ for 16 h, EtOH was removed *in vacuo*. The residue was washed with water and extracted with CH_2Cl_2. The organic layer was dried over anhydrous $MgSO_4$ and the solvent was removed *in vacuo* to give the crude product. Purification by flash column chromatography (silica gel, petroleum ether/CH_2Cl_2 1:4) gave **3b** as a blue powder (600 mg, 35%). ^{1}H NMR (400 MHz, $CDCl_3$) δ 8.12 (d, *J* = 15.2 Hz, 1H, Ar'-CH=C), 8.05 (d, *J* = 7.5 Hz, 2H, Ar-H), 7.62 (t, *J* = 7.4 Hz, 1H, Ar-H), 7.56 (d, *J* = 8.9 Hz, 2H, Ar'-H), 7.51 (t, *J* = 7.7 Hz, 2H, Ar-H), 6.71 (d, *J* = 8.9 Hz, 2H, Ar'-H), 6.57 (d, *J* =

15.2 Hz, 1H, CH=CH(CO)), 6.53 (s, 1H, (CO)CH(CO)), 3.11 (s, 6H, CH_3). ^{13}C NMR (100 MHz, $CDCl_3$) δ 180.99, 178.86, 153.31, 149.67, 133.92, 132.72, 132.18, 130.91, 129.93, 128.90, 128.55, 128.28, 127.14, 121.91, 114.16, 111.98, 97.06, 40.14. HRMS (ESI) m/z calcd for $C_{19}H_{18}BF_2NNaO_2$ $[M+Na]^+$ 364.12943, found 364.12937.

2.2.9 Synthesis of **3c**

3c was synthesized from **3b** by the same method as **1c**. Purification by flash column chromatography (silica gel, petroleum ether/CH_2Cl_2 1:2) gave **3c** as a dark blue powder. Yield 42%. ^{1}H NMR (400 MHz, $CDCl_3$) δ 8.12 (d, *J* = 14.8 Hz, 1H, Ar'-CH=C), 7.97 (d, *J* = 7.4 Hz, 2H, Ar-H), 7.68 – 7.56 (m, 3H), 7.51 (t, *J* = 7.8 Hz, 2H, Ar-H), 6.73 (d, *J* = 9.0 Hz, 2H, Ar'-H), 6.58 – 6.49 (m, 2H), 3.17 (s, 6H, CH_3). ^{13}C NMR (100 MHz, $CDCl_3$) δ 178.91, 176.01, 154.50, 153.07, 134.59, 133.81, 131.72, 129.11, 128.36, 121.98, 112.44, 112.34, 99.14, 40.27. HRMS (ESI) m/z calcd for $C_{21}H_{18}BN_3NaO_2$ $[M+Na]^+$ 378.13788, found 378.13880.

2.3 Fluorescence quantum yields measurement

The fluorescence quantum yields *Φ* were calculated from the relation shown in the following equation:

$$\Phi_u = \Phi_s \times (F_u/A_u) \times (A_s/F_s) \times (n_u^2/n_s^2)$$

in which u and s denote a dye and a standard, respectively, *A* is the absorbance at the excitation wavelength, *F* is the integrated emission area, and *n* is the refractive index for the solvent [18].

Fluorescence quantum yields, Φ_f, for β-diketonate derivatives (**1b**, **1c**, **2b**, **2c**) in

CH_2Cl_2 were calculated *versus* anthracene in EtOH as a standard method using the following values: Φ_f(anthracene) =0.27, n_D^{20}(EtOH) = 1.360, and n_D^{20}(CH_2Cl_2) = 1.424 [19,20]. Optically dilute CH_2Cl_2 solutions of β-diketonate derivatives and EtOH solutions of the anthracene standard were prepared in 1 cm path length quartz cuvettes with absorbances < 0.1. Quantum yield measurements were performed with excitation at λ_{ex} = 356 nm and emission integration range = 370-700 nm. Fluorescence quantum yields for β-diketonate derivatives (**3b**, **3c**) in CH_2Cl_2 were calculated *versus* rhodamine B in EtOH as a standard method using the following values: Φ_f (rhodamine B) =0.5, n_D^{20}(EtOH) = 1.360, and n_D^{20}(CH_2Cl_2) = 1.424 [19,20]. Optically dilute CH_2Cl_2 solutions of β-diketonate derivatives and EtOH solutions of the rhodamine B standard were prepared in 1 cm path length quartz cuvettes with absorbances < 0.1. Quantum yield measurements were performed with excitation at λ_{ex} = 500 nm and an emission integration range = 520-750 nm.

2.4 Cell culture and cell imaging

HeLa cells were cultured in Dulbecco's Modified Eagle's Medium (DMEM), supplemented with 10% Fetal Bovine Serum (FBS), penicillin (100 units/mL), and streptomycin (100 μg/mL) at 37 °C in a humidified atmosphere of 5% CO_2 for 24 h. The cells were seeded in a glass-bottom cell culture dish (NEST Biotechnology Co. LTD.) and incubated with 1 μM compound **3c** at 37 °C in a humidified atmosphere of 5% CO_2 for 6 h, then were replaced three times with fresh growth medium. Confocal cell imaging was performed on a Nikon Eclipse Ti confocal laser scanning microscopy (CLSM) with a TDKAI HIT live cell imaging system. Fluorescence was

excited at 561 nm and emission was collected by a 570-620 nm band pass filter.

3. Results and Discussion

3.1 Synthesis and Characterization

The Claisen condensation reaction of acetophenone and benzoate gave the ligands **1a**-**2a** (Scheme S1 in supplementary data) [17], which exist as their enol forms in solution as indicated by the ^{1}H NMR. **1a**-**2a** were then allowed to react with the boron trifluoride-diethyl ether complex in the presence of triethylamine in dichloromethane to afford the corresponding BF_2 complexes **1b**-**2b**. The $B(CN)_2$ (**1c**, **2c**, **3c**) were synthesized by treatment of the corresponding difluoroboron diketonates (**1b**, **2b**, **3b**) with trimethylsilyl cyanide (TMSCN) in the presence of boron trifluoride diethyl etherate in CH_2Cl_2 at room temperature (Scheme 2). The successful substitutions were confirmed by ^{1}H and ^{13}C NMR, IR and HRMS (see supplementary data).

Scheme 2. Synthesis of dicyanoboron diketonate complexes.

3.2 Optical Properties

Figure 1. (a) UV-vis absorption and (b) normalized fluorescence spectra of **1b**-**3b**, **1c**-**3c** in dichloromethane (1.0×10^{-5} M).

Table 1. Photophysical Properties of Difluoroboron Diketonates and Dicyanoboron Diketonates.

compd	in dichloromethane[a]							solid state	Energy
	λ_{max} [nm] (ε)	F_{max}[b] [nm]	Stokes shift [nm]	Φ_f[b,c]	τ_s[d] [ns]	k_f[e] [10^9 s^{-1}]	k_{nr}[f] [10^9 s^{-1}]	F_{max}[g] [nm]	gap_{calc} [eV]
1b	412 (78200)	438	26	0.85	2.15	0.40	0.07	501	3.7144
1c	439 (78500)	464	25	0.66	2.23	0.30	0.15	547	3.5076
2b	411 (63200)	438	27	0.72	1.96	0.37	0.14	501	3.6409
2c	440 (69700)	466	26	0.24	2.05	0.12	0.37	550	3.4123
3b	535 (87800)	621	86	0.026	0.51	0.05	1.91	——[h]	3.0287
3c	585 (97600)	664	79	<0.001[h]	1.43	<0.001[h]	0.70	——[h]	2.8491

[a] Measured at a concentration of 1.0×10^{-5} mol dm^{-3}. [b] The excitation wavelengths (λ_{ex}) were as follows: **1b** (**c**) (356 nm), **2b** (**c**) (356 nm), **3b** (450 nm) and **3c** (530 nm). [c] Φ_f is the relative fluorescence quantum yield estimated using anthracene (Φ_f = 0.27 in ethanol) for **1b**, **1c**, **2b**, **2c** or rhodamine B (Φ_f = 0.5 in ethanol) for **3b**-**3c** as standard. [d] Measured using time-resolved fluorescence measurements. [e] Radiative rate constant ($k_f = \Phi_f/\tau_f$). [f] Nonradiative rate constant ($k_{nr} = (1 - \Phi_f)/\tau_f$). [g] The λ_{ex} were as follow: **1b** (410 nm), **1c** (440 nm), **2b** (410 nm), **2c** (440 nm). [h] Too weak to be measured.

To examine the optical properties of the obtained boron dicyanodiketonates, UV-vis absorption and emission spectra were carried out in CH_2Cl_2 (Figure 1). The data are compared to those of the model BF_2 complexes **1b**-**3b** (Table 1). Substitution of fluorine by cyano group strongly influences the absorption and emission spectra. **1c**-**3c** exhibited strong absorption (ε > 60000 M^{-1} cm^{-1}) in the 440-580 nm region, which are red-shifted > 25 nm compared to those of BF_2 complexes. Especially in **3c**,

the absorption maxima shifted as much as 43 nm compared to that of **3b**. The molar absorption coefficients of $B(CN)_2$ complexes are generally higher than those of the BF_2 compounds. The emission maxima of $B(CN)_2$ complexes are red-shifted proportionally with the absorption changes. In other words, the Stokes shift didn't change much after cyano substitution.

As shown in Table 1, the organoboron BF_2 dyes **1b** and **2b** are highly emissive, with fluorescence quantum yields in CH_2Cl_2 at room temperature are 0.85 and 0.72, respectively. After substitution with cyano group, the quantum yields of **1c** and **2c** decrease to 0.66 and 0.24. In light of the fact that the nonradiative rate constants (k_{nr}) of **1c** (0.15×10^9 s^{-1}) and **2c** (0.37×10^9 s^{-1}) are higher compared with those of **1b** (0.07×10^9 s^{-1}) and **2b** (0.14×10^9 s^{-1}), there may be other processes in the nonradiative decay of $B(CN)_2$ compounds responsible for the lower quantum yields [21,22].

The absorption and emission of **3b** and **3c** in CH_2Cl_2 are in the deep red region due to their more extensive π conjugation and the presence of intramolecular charge transfer (ICT) process. The molar absorption coefficient (ε) of **3c** is significantly higher than those of **1b** (**c**) and **2b** (**c**), which might be due to the extension of π conjugation and the two substituted cyano groups. Very weak fluorescence was observed for **3b** and **3c** in CH_2Cl_2 for reasons to be discussed below. The Stokes shifts for **3b** and **3c** are as large as 86 nm, which implies that there is a large difference in the molecular structures between the ground and excited states. The presence of ICT process is indicated [23]. The excitation spectra of **3b** and **3c** almost match well with their absorption spectra. (Figure S1)The emission of $B(CN)_2$ complexes (**1c** and **2c**)

were red-shifted 84 nm in their solid state with respect to those in solution, while the emission of BF_2 complexes (**1b** and **2b**) in the solid state were red shifted 63 nm compared with those in solution. These changes might be due to different packing structures in the solids with different substituents for the BF_2 and $B(CN)_2$ complexes. Fluorescence of **3b** and **3c** in the solid state was too weak to be observed.

3.3 Solvent Effects

Dye emission color tuning can also take advantage of solvatochromism. Polar dyes in particular can be sensitive to the properties of their surroundings. The polarity or dielectric constant of the local medium can affect the ground state or excited state energies of fluorophores or both. To demonstrate the solvent effect, the absorption and emission of **3b** and **3c** in different solvents were measured (Figure 2, Table 2 and 3). The absorption spectra of **3b** and **3c** show minor changes in different solvents, which suggests that the difference among their ground-state dipole moments in different solvents is rather small. However, the color changes of **3b** and **3c** in different solvents could easily be visualized by naked-eye (Figure S2 and S3). For example, the color of **3c** changed from pink to blue when the solvent was changed from toluene to acetonitrile. The fluorescence emission spectra of **3b** and **3c** exhibit positive solvatochromism in general. The fluorescence quantum yields of **3b** and **3c**, which are high in toluene (0.5 and 0.28 respectively), are too low to be determined in the more polar solvent such as methanol.

Typically, the fluorescence emission spectra from an ICT state are very dependent on the polarity of solvents [24]. The fluorescence quantum yields are low in polar

solvents but high in low polarity ones. Consequently, the presence of an ICT process in **3b** and **3c** was indicated. Kinetic constants were also determined for radiative and nonradiative deactivation pathways in various solvents and are collected in Table 2 and Table 3. The radiative constants k_f of **3b** and **3c** are found to decrease with the polarity of solvents, accompanied by an increase of the nonradiative constant k_{nr}. According to the energy gap rule [25], this decrease in fluorescence quantum yield (Φ_f) and lifetime (τ_s) is attributed to the acceleration of internal conversion (ic) as the energy gap between the excited and the ground state decreases. Thus, the observed positive solvato-kinetic effect does not arise from the population of different emitting species during the lifetime of the excited state, but the quenching of the highly polar ICT state which is caused by an increase of k_{ic}.

Figure 2. Fluorescence spectra of **3b** (a) and **3c** (b) in various solvents (1.0×10^{-5} M).

Table 2. Absorption and Emission Properties of **3b** in Various Solvents.

solvent[a]	Δf[b]	λ_{max} [nm] (ε)	F_{max}[c] [nm]	Stokes shift [nm/cm^{-1}]	Φ_f[d]	τ_s[e] [ns]	k_f[f] [10^9 s^{-1}]	k_{nr}[g] [10^9 s^{-1}]
Toluene	0.02	519 (62400)	573	54/1820	0.50	2.42	0.21	0.21
$CHCl_3$	0.15	530 (72600)	600	70/2200	0.17	2.55	0.07	0.33
THF	0.21	522 (71200)	611	89/2790	0.024	0.52	0.05	1.88
CH_2Cl_2	0.22	535 (87800)	621	86/2590	0.026	0.51	0.05	1.91
Acetone	0.28	530 (69500)	582	52/1690	<0.001[h]	1.97	<0.001[h]	0.51
CH_3OH	0.30	528 (63400)	612	84/2600	<0.001[h]	0.35	<0.001[h]	2.86
CH_3CN	0.31	535 (66600)	593	58/1830	<0.001[h]	1.26	<0.001[h]	0.79

[a] Measured at a concentration of 1.0×10^{-5} mol dm^{-3}. [b] Solvent polarity parameter ($[(\varepsilon - 1)/(2\varepsilon + 1)] - [(n^2 -$

1)/(2n^2 + 1)]) (ref 23). [c] The excitation wavelengths (λ_{ex}) is 450 nm in all solvents. [d] Φ_f is the relative fluorescence quantum yield estimated by using rhodamine B (Φ_f = 0.5 in ethanol) as standard. [e] Measured using time-resolved fluorescence measurements. [f] Radiative rate constant ($k_f = \Phi_f/\tau_f$). [g] Nonradiative rate constant ($k_{nr} = (1 - \Phi_f)/\tau_f$). [h] Too weak to be measured.

Table 3. Absorption and Emission Properties of **3c** in Various Solvents.

solvent[a]	Δf[b]	λ_{max} [nm] (ε)	F_{max}[c] [nm]	Stokes shift [nm/cm^{-1}]	Φ_f[d]	τ_s[e] [ns]	k_f[f] [10^9 s^{-1}]	k_{nr}[g] [10^9 s^{-1}]
Toluene	0.02	572 (104400)	624	52/1457	0.28	2.53	0.11	0.28
$CHCl_3$	0.15	580 (107700)	639	59/1592	0.021	0.63	0.03	1.55
THF	0.21	580 (92700)	659	79/2067	0.002	1.42	0.001	0.70
CH_2Cl_2	0.22	585 (97600)	664	79/2034	<0.001[h]	1.43	<0.001[h]	0.70
Acetone	0.28	585 (96100)	667	82/2102	<0.001[h]	1.99	<0.001[h]	0.50
CH_3OH	0.30	586 (93100)	665	79/2027	<0.001[h]	0.61	<0.001[h]	1.64
CH_3CN	0.31	586 (92500)	675	89/2250	<0.001[h]	1.30	<0.001[h]	0.77

[a] Measured at a concentration of 1.0 × 10^{-5} mol dm^{-3}. [b] Solvent polarity parameter ([(ε − 1)/(2ε + 1)] − [(n^2 − 1)/(2n^2 + 1)]). [c] The excitation wavelengths (λ_{ex}) is 530 nm in all solvents. [d] Φ_f is the relative fluorescence quantum yield estimated by using rhodamine B (Φ_f = 0.5 in ethanol) as standard. [e] Measured using time-resolved fluorescence measurements. [f] Radiative rate constant ($k_f = \Phi_f/\tau_f$). [g] Nonradiative rate constant ($k_{nr} = (1 - \Phi_f)/\tau_f$). [h] Too weak to be measured.

3.4 Theoretical Calculations

The Gaussian 03 software package [26] was used for all computational modeling. The geometries for **1b-3b** and **1c-3c** were optimized with a density functional theory (DFT) method, using the B3LYP//6-311+G* basis set. Figure 3 shows the lowest unoccupied molecular orbital (LUMO) and the highest occupied molecular orbital

(HOMO) for **1b**-**3b**, **1c**-**3c**. The corresponding energy gaps between LUMO and HOMO are included in Table 1.

The substitution of fluorine by cyano group in the boron diketonates did not change the location of the π orbital of the 1,3-diketone group. As a result, the transition between the excited state and ground state is allowed because the π,π* excited states of these six compounds occupy the lowest excited state. In contrast, the bathochromic shift experimentally observed for $B(CN)_2$ complexes after cyano substitution can be attributed to more pronounced lowering of the LUMO rather than elevation of the HOMO. On the other hand, as indicated by the DFT calculations, extended conjugation in **3b** and **3c** leads to elevation of the HOMO levels and thus the observed bathochromic shift of the emission compared with **1b** (**c**) and **2b** (**c**) .

Figure 3. Calculated molecular orbital energy diagram and isodensity surface plots of the frontier orbitals (HOMO and LUMO) of **1b**-**3b**, **1c**-**3c**.

3.5 Confocal Fluorescent Images of Cells

Fluorescence probes are useful for imaging various biological functions and diagnostic application. Considering the promising biological applications, some cell-imaging experiments of **3c** were conducted. In our experiment, HeLa cells were incubated with **3c** at the concentration of 1 μM for 6 h. We chose this dye because its deep red fluorescence had minimal interference from background autofluorescence of the cells. It is apparent from Figure 4 that **3c** could readily penetrate cell membranes,

and the strong intracellular fluorescence may be attributed to the distribution of the dyes in the lipophilic environment of the cytoplasm. Although **3c** shows almost no fluorescence (Φ < 0.001) in polar solvents, the fluorescence intensity in cytoplasm was sufficient to provide strong contrast for imaging due to its possible enrichment inside the low polarity microenvironment of cytoplasm. Almost no background fluorescence could be observed.

Figure 4. Confocal fluorescence images of living HeLa cells: (a) bright field image of living HeLa cells; (b) fluorescence image of living HeLa cells incubated with 1 μM **3c** for 6 h; (c) the overlap of bright field and fluorescence images.

For a fluorescence probe to be of practical value, photostability is very important because of the possible temporal monitoring of dynamic events inside cells. To evaluate the photostability of the probe, the deep red dyes **3b** and **3c** were irradiated in toluene continuously at λ > 420 nm using a 500 W Xe lamp as the collimated light source. As monitored by UV spectra, the absorption intensity of **3c** could keep 93% at 567 nm after 15 min continuous irradiation, while the intensity of **3b** dropped to 85% (Figure 5). This indicates that the photostability of the cyano group substituted boron diketonates derivatives is much higher than that of BF_2 compounds. The cytotoxicity of **3c** in HeLa cells was examined using the Cell Counting Kit-8 (CCK-8) assay. The results indicate that **3c** has low cytotoxicity (cell viability > 95%) after incubation for 4 hours, even at 10 μM (Figure S4 in supplementary data).

Figure 5. Photostability of **3b** and **3c** (1.0×10^{-5} M) in toluene.

4. Conclusions

In summary, we have synthesized a new class of dicyanoboron diketonates from difluoroboron diketonate derivatives. Dicyanoboron diketonates show relatively high molar absorption coefficients (> 60000 M^{-1} cm^{-1}) and larger red-shifts (> 25 nm) in their absorption and emission spectra than do the corresponding difluoroboron diketonates. Especially, the fluorescence emission wavelength of **3c** extended to the deep red region (664 nm in CH_2Cl_2). The emission of **3b** and **3c** are very sensitive to the polarity of solvents. The fluorescence quantum yields of **3b** and **3c** are reasonably high in low polarity solvents, but too low to be determined in high polarity solvents. Cell imaging experiments demonstrated the potential application of **3c** as a probe in bioorganisms due to its good imaging contrast, large Stokes shift, low cytotoxicity and high photostability. This strategy represents a facile approach to modulate the photophysical properties of dyes.

Acknowledgments

This work was financially supported by the National Natural Science Foundation of China (21272243, 21102155, 91027041) and the 973 Program (2013CB933800). We thank Dr. Ye Tian (TIPC, CAS) for her help in cell imaging and Dr. Man Wu (TIPC, CAS) for her help in the cytotoxicity test.

Appendix A. Supplementary data

Absorption spectra of **3b** and **3c** in various solvents; Cytotoxicity; Synthetic route for **1a** and **2a**; ^{1}H NMR, ^{13}C NMR, MS-EI , HRMS-ESI and FT-IR spectra of **1a**-**3c**. Supplementary data related to this article can be found at http://dx.doi.org/10.1016/xxx.

References

[1] (a) Loudet A, Burgess K. BODIPY Dyes and Their Derivatives: Syntheses and Spectroscopic Properties. Chem Rev 2007;107(11):4891-932.

(b) Kamkaew A, Lim SH, Lee HB, Kiew LV, Chung LY, Burgess K. BODIPY dyes in photodynamic therapy. Chem Soc Rev 2013;42(1):77-88.

(c) Boens N, Leen V, Dehaen W. Fluorescent indicators based on BODIPY. Chem Soc Rev 2012;41(3):1130-72.

(d) Wade CR, Broomsgrove AEJ, Aldridge S, Gabbaı FoP. Fluoride Ion Complexation and Sensing Using Organoboron Compounds. Chem Rev 2010;110:3958-84.

(e) Benniston AC, Copley G. Lighting the way ahead with boron dipyrromethene (Bodipy) dyes. Phys Chem Chem Phys 2009;11(21):4124-31.

[2] Zhai D, Lee SC, Yun SW, Chang YT. A ratiometric fluorescent dye for the detection of glutathione in live cells and liver cancer tissue. Chem Commun 2013;49(65):7207-9.

[3] Zhang HX, Chen JB, Guo XF, Wang H, Zhang HS. Highly sensitive low-background fluorescent probes for imaging of nitric oxide in cells and tissues. Anal Chem 2014;86(6):3115-23.

[4] Zhang G, Palmer GM, Dewhirst MW, Fraser CL. A dual-emissive-materials design concept enables tumour hypoxia imaging. Nat Mater 2009;8(9):747-51.

[5] Liu W, Li F, Chen X, Hou J, Yi L, Wu YW. A Rapid and Fluorogenic TMP-AcBOPDIPY Probe for

Covalent Labeling of Proteins in Live Cells. J Am Chem Soc 2014;136(12):4468-71.

[6] (a) Karakus E, Ucuncu M, Emrullahoglu M. A rhodamine/BODIPY-based fluorescent probe for the differential detection of Hg(II) and Au(III). Chem Commun 2014;50(9):1119-21.

(b) Madhu S, Ravikanth M. Boron-dipyrromethene based reversible and reusable selective chemosensor for fluoride detection. Inorg Chem 2014;53(3):1646-53.

(c) P CA, Thilagar P. Triarylborane-appended new triad and tetrad: chromogenic and fluorogenic anion recognition. Inorg Chem 2014;53(6):2776-86.

[7] Garcı´a-Moreno I, Costela A, Campo L, Sastre R, Amat-Guerri F, Liras M, et al. 8-Phenyl-Substituted Dipyrromethene • BF_2 Complexes as Highly Efficient and Photostable Laser Dyes. J Phys Chem A 2004;108:3315-23.

[8] García-Moreno I, Amat-Guerri F, Liras M, Costela A, Infantes L, Sastre R, et al. Structural Changes in the BODIPY Dye PM567 Enhancing the Laser Action in Liquid and Solid Media. Adv Funct Mater 2007;17(16):3088-98.

[9] Xu S, Evans RE, Liu T, Zhang G, Demas JN, Trindle CO, et al. Aromatic difluoroboron β-diketonate complexes: effects of π-conjugation and media on optical properties. Inorg Chem 2013;52(7):3597-610.

[10] Zhang G, Chen J, Payne SJ, Kooi SE, Demas JN, Fraser CL. Multi-Emissive Difluoroboron Dibenzoylmethane Polylactide Exhibiting Intense Fluorescence and Oxygen-Sensitive Room-Temperature Phosphorescence. J Am Chem Soc 2007;129:8942-3.

[11] (a) Mayoral MJ, Ovejero P, Cano M, Orellana G. Alkoxy-substituted difluoroboron benzoylmethanes for photonics applications: a photophysical and spectroscopic study. Dalton Trans 2011;40(2):377-83.

(b) Zhang G, Kooi SE, Demas JN, Fraser CL. Emission Color Tuning with Polymer Molecular Weight for Difluoroboron Dibenzoylmethane-Polylactide. Adv Mater 2008;20(11):2099-104.

(c) Yoshii R, Nagai A, Tanaka K, Chujo Y. Highly emissive boron ketoiminate derivatives as a new class of aggregation-induced emission fluorophores. Chem Eur J 2013;19(14):4506-12.

(d) Wang DJ, Kang YF, Xu BP, Zheng J, Wei XH. Synthesis, characterization and fluorescence properties of boron difluoride pyridyl-β-diketonate derivatives. Spectrochim Acta A Mol Biomol Spectrosc 2013;104:419-22.

(e) Kumar GR, Thilagar P. Triarylborane conjugated acacH ligands and their BF_2 complexes: facile synthesis and intriguing optical properties. Dalton Trans 2014;43(10):3871-9.

[12] (a) Sanchez-Carnerero EM, Moreno F, Maroto BL, Agarrabeitia AR, Ortiz MJ, Vo BG, et al. Circularly Polarized Luminescence by Visible-Light Absorption in a Chiral O-BODIPY Dye: Unprecedented Design of CPL Organic Molecules from Achiral Chromophores. J Am Chem Soc 2014;136(9):3346-9.

(b) Rohand T, Baruah M, Qin W, Boens N, Dehaen W. Functionalisation of fluorescent BODIPY dyes by nucleophilic substitution. Chem Commun 2006(3):266-8.

(c) Kubota Y, Ozaki Y, Funabiki K, Matsui M. Synthesis and fluorescence properties of pyrimidine mono- and bisboron complexes. J Org Chem 2013;78(14):7058-67.

(d) Zhao C, Feng P, Cao J, Zhang Y, Wang X, Yang Y, et al. 6-Hydroxyindole-based borondipyrromethene: synthesis and spectroscopic studies. Org Biomol Chem 2012;10(2):267-72.

(e) Boens N, Wang L, Leen V, Yuan P, Verbelen B, Dehaen W, et al. 8-HaloBODIPYs and Their 8-(C, N, O, S) Substituted Analogues: Solvent Dependent UV-Vis Spectroscopy, Variable Temperature NMR, Crystal Structure Determination, and Quantum Chemical Calculations. J Phys

Chem A 2014;118(9):1576-94.

(f) Hao Q., Yu S., Li S., Chen J., Zeng Y., Yu T., Yang G., Li Y. Locked Planarity: A Strategy for Tailoring Ladder-Type π-Conjugated Anilido–Pyridine Boron Difluorides. J. Org. Chem., 2014, 79 (1): 459–464.

[13] Chen J, Liu W, Zhou B, Niu G, Zhang H, Wu J, et al. Coumarin- and rhodamine-fused deep red fluorescent dyes: synthesis, photophysical properties, and bioimaging in vitro. J Org Chem 2013;78(12):6121-30.

[14] (a) Goeb Sb, Ziessel R. Convenient Synthesis of Green Diisoindolodithienylpyrromethene-Dialkynyl Borane Dyes. Org Lett 2007;9(5):737-40.

(b) Li L, Nguyen B, Burgess K. Functionalization of the 4,4-difluoro-4-bora-3a,4a-diaza-s-indacene (BODIPY) core. Bioorg Med Chem Lett 2008;18(10):3112-6.

(c) Nagai A, Miyake J, Kokado K, Nagata Y, Chujo Y. Highly Luminescent BODIPY-Based Organoboron Polymer Exhibiting Supramolecular Self-Assemble Structure. J Am Chem Soc 2008;130(46):15276-8.

(d) Ulrich G, Goze C, Goeb Sb, Retailleau P, Ziessel R. New fluorescent aryl- or ethynylaryl-boron-substituted indacenes as promising dyes. New J Chem 2006;30(7):982.

(e) Goze C, Ulrich G, Mallon LJ, Allen BD, Harriman A, Ziessel R. Synthesis and Photophysical Properties of Borondipyrromethene Dyes Bearing Aryl Substituents at the Boron Center. J Am Chem Soc 2006;128(31):10231-9.

(f) Bonardi L, Ulrich G, Ziessel R. Tailoring the Properties of Boron-Dipyrromethene Dyes with Acetylenic Functions at the 2,6,8 and 4-B Substitution Positions. Org Lett 2008;10(11):2183-6.

(g) Goze C, Ulrich G, Ziessel R. Tetrahedral Boron Chemistry for the Preparation of Highly Efficient “Cascatelle” Devices. J Org Chem 2007;72(2):313-22.

(h) Goze C, Ulrich G, Ziessel R. Unusual Fluorescent Monomeric and Dimeric Dialkynyl Dipyrromethene-Borane Complexes. Org Lett 2006;8(20):4445-8.

[15] (a) Nagai A, Kokado K, Nagata Y, Arita M, Chujo Y. Highly Intense Fluorescent Diarylboron Diketonate. J Org Chem 2008;73:8605-7.

(b) Kubota Y, Hara H, Tanaka S, Funabiki K, Matsui M. Synthesis and Fluorescence Properties of Novel Pyrazine-Boron Complexes Bearing a β-Iminoketone Ligand. Org Lett 2011;13(24):6544-7.

(c) Poon C-T, Lam WH, Yam VW-W. Synthesis, Photochromic, and Computational Studies of Dithienylethene-Containing β-Diketonate Derivatives and Their Near-Infrared Photochromic Behavior Upon Coordination of a Boron(III) Center. Chem Eur J 2013;19(10):3467-76.

(d) Nagai A, Kokado K, Nagata Y, Chujo Y. 1,3-Diketone-Based Organoboron Polymers: Emission by Extending π-Conjugation along a Polymeric Ligand. Macromolecules 2008;41:8295-8.

[16] (a) Xin L, Chen YZ, Niu LY, Wu LZ, Tung CH, Tong QX, et al. A selective turn-on fluorescent probe for Cd^{2+} based on a boron difluoride beta-dibenzoyl dye and its application in living cells. Org Biomol Chem 2013;11(18):3014-9.

(b) Niu LY, Guan YS, Chen YZ, Wu LZ, Tung CH, Yang QZ. A turn-on fluorescent sensor for the discrimination of cystein from homocystein and glutathione. Chem Commun 2013;49(13):1294-6.

(c) Niu LY, Guan YS, Chen YZ, Wu LZ, Tung CH, Yang QZ. BODIPY-based ratiometric fluorescent sensor for highly selective detection of glutathione over cysteine and homocysteine. J

Am Chem Soc 2012;134(46):18928-31.

[17] Sun X, Zhang X, Li X, Liu S, Zhang G. A mechanistic investigation of mechanochromic luminescent organoboron materials. J Mater Chem 2012;22(33):17332.

[18] Resch-Genger U, Rurack K. Determination of the photoluminescence quantum yield of dilute dye solutions (IUPAC Technical Report). Pure Appl Chem 2013;85(10).

[19] Brouwer AM. Standards for photoluminescence quantum yield measurements in solution (IUPAC Technical Report). Pure Appl Chem 2011;83(12).

[20] Weast RC and Astle MJ. CRC Handbook of Data on Organic Compounds, Vol. I and II. CRC Press 1985.

[21] Caldwell RA, Jacobs LD, Furlani TR, Nalley EA, Laboy J. Conformationally Dependent Heavy Atom Effect of Chlorine on Alkene Triplet Lifetimes. Experimental and ab Initio Calculations. J Am Chem Soc 1992;114:1623-5.

[22] Gorman A, Killoran J, Shea CO, Kenna T, Gallagher WM, Shea DFO. In Vitro Demonstration of the Heavy-Atom Effect for Photodynamic Therapy. J Am Chem Soc 2004;126:10619-31.

[23] Rurack K, Kollmannsberger M, Daub J. Molecular Switching in the Near Infrared (NIR) with a Functionalized Boron-Dipyrromethene Dye. Angew Chem Int Ed 2001;40:385-7.

[24] (a) Moyon NS, Mitra S. Fluorescence solvatochromism in lumichrome and excited-state tautomerization: a combined experimental and DFT study. J Phys Chem A 2011;115(12):2456-64.

(b) Hu R, Lager E, Aguilar-Aguilar Al, Liu J, Lam JWY, Sung HHY, et al. Twisted Intramolecular Charge Transfer and Aggregation-Induced Emission of BODIPY Derivatives. J phys Chem C 2009;113:15845-53.

[25] Wardle B. Principles and Applications of Photochemistry. Wiley 2009.

[26] Frisch MJ, Trucks GW, Schlegel HB, Scuseria GE, Robb MA, Cheeseman JR, Montgomery JAJ, Vreven T, Kudin KN, Burant JC, Millam JM, Iyengar SS, Tomasi J, Barone V, Mennucci B, Cossi M, Scalmani G, Rega N, Petersson GA, Nakatsuji H, Hada M, Ehara M, Toyota K, Fukuda R, Hasegawa J, Ishida M, Nakajima T, Honda Y, Kitao O, Nakai H, Klene M, Li X, Knox JE, Hratchian HP, Cross JB, Bakken V, Adamo C, Jaramillo J, Gomperts R, Stratmann RE, Yazyev O, Austin AJ, Cammi R, Pomelli C, Ochterski JW, Ayala PY, Morokuma K, Voth GA, Salvador P, Dannenberg JJ, Zakrzewski VG, Dapprich S, Daniels AD, Strain MC, Farkas O, Malick DK, Rabuck AD, Raghavachari K, Foresman JB, Ortiz JV, Cui Q, Baboul AG, Clifford S, Cioslowski J, Stefanov BB, Liu G, Liashenko A, Piskorz P, Komaromi I, Martin RL, Fox DJ, Keith T, Al-Laham MA, Peng CY, Nanayakkara A, Challacombe M, Gill PMW, Johnson B, Chen W, Wong MW, Gonzalez C, Pople JA. Gaussian 03, Gaussian Inc., Wallingford CT, 2004.

Captions

Scheme 1. Structures of the difluoroboron diketonates **1b**-**3b** and dicyanoboron diketonates **1c**-**3c**.

Scheme 2. Synthesis of dicyanoboron diketonate complexes.

Figure 1. (a) UV-vis absorption and (b) normalized fluorescence spectra of **1b**-**3b**, **1c**-**3c** in dichloromethane (1.0×10^{-5} M).

Figure 2. Fluorescence spectra of **3b** (a) and **3c** (b) in various solvents (1.0×10^{-5} M).

Figure 3. The calculated molecular orbital energy diagram and isodensity surface plots of the frontier orbitals (HOMO and LUMO) of **1b**-**3b**, **1c**-**3c**.

Figure 4. Confocal fluorescence images of living HeLa cells: (a) bright field image of living HeLa cells; (b) fluorescence image of living HeLa cells incubated with 1 μM **3c** for 6 h; (c) the overlap of bright field and fluorescence images.

Figure 5. Photostability of **3b** and **3c** (1.0×10^{-5} M) in toluene.

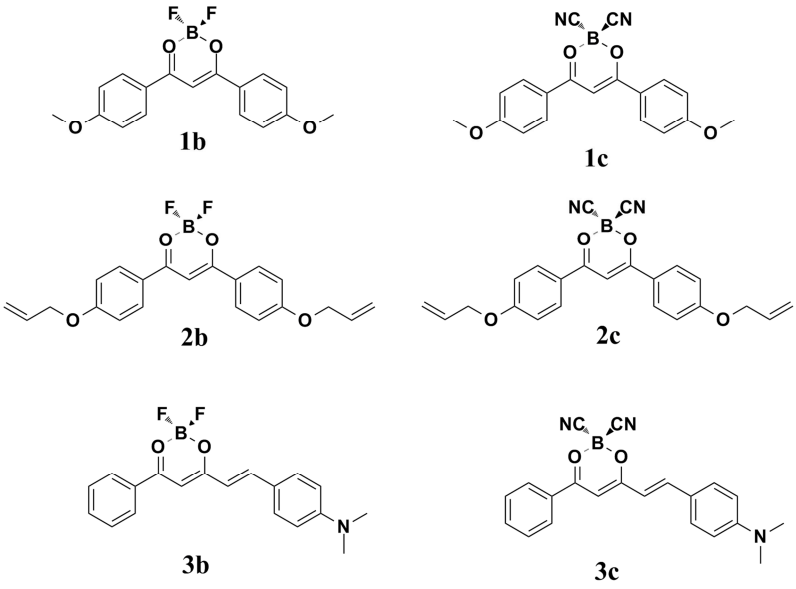

Scheme 1

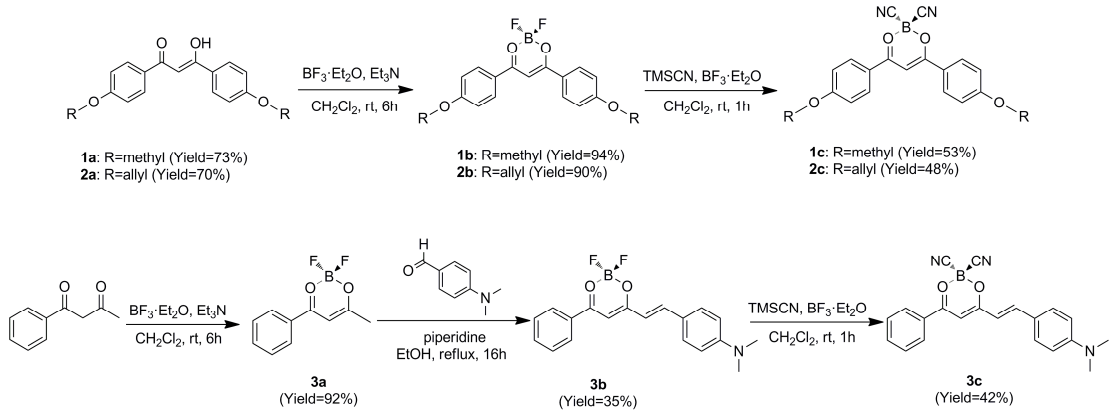

Scheme 2

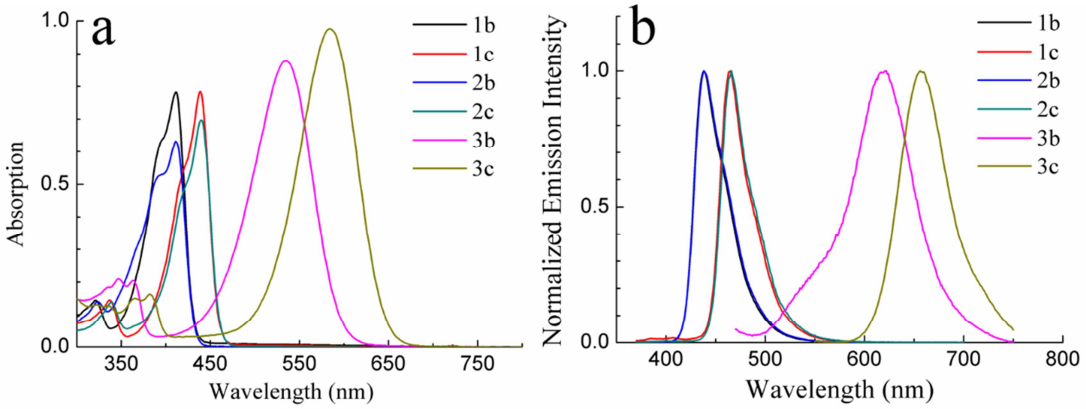

Figure 1

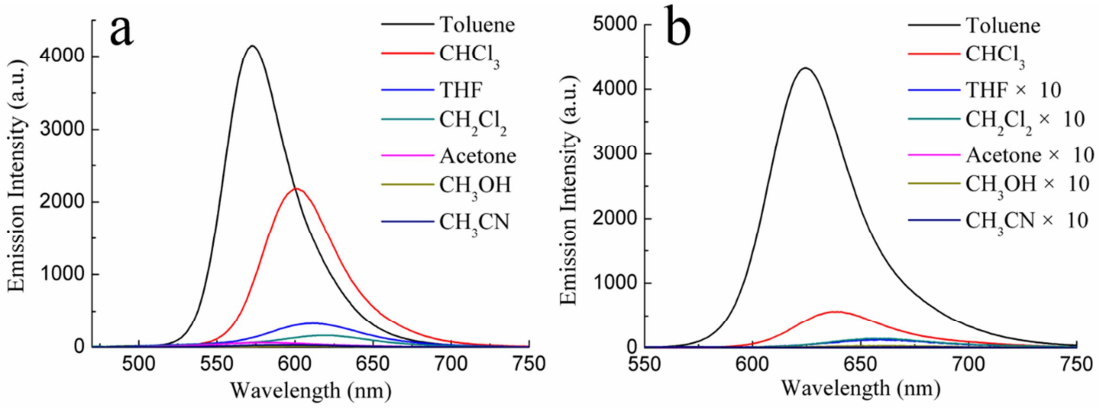

Figure 2

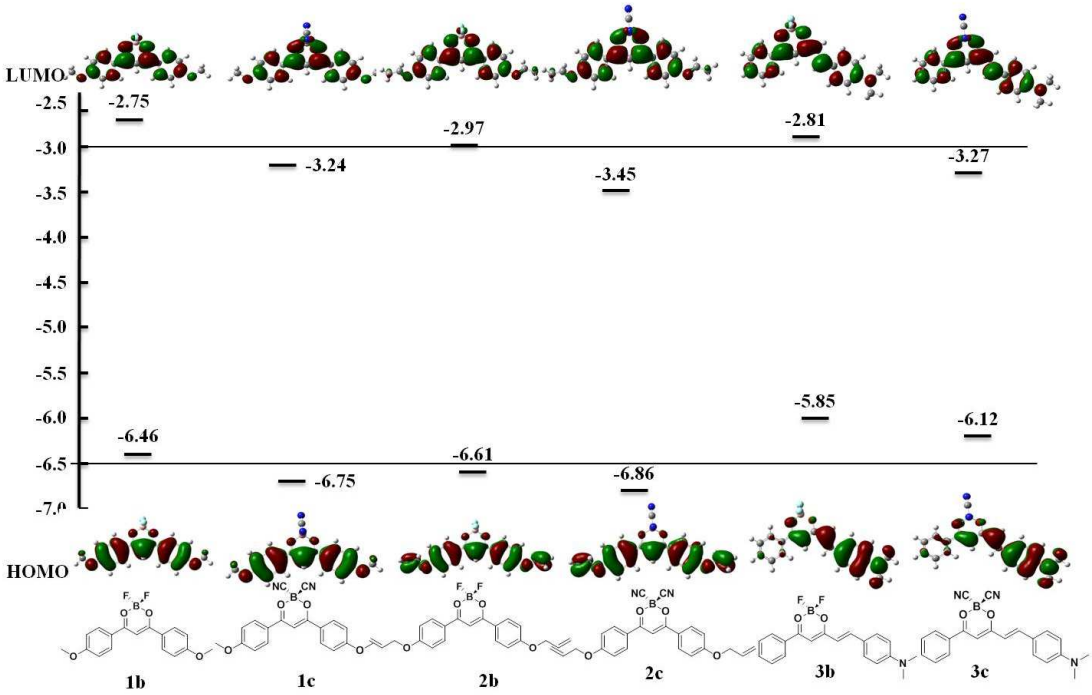

Figure 3

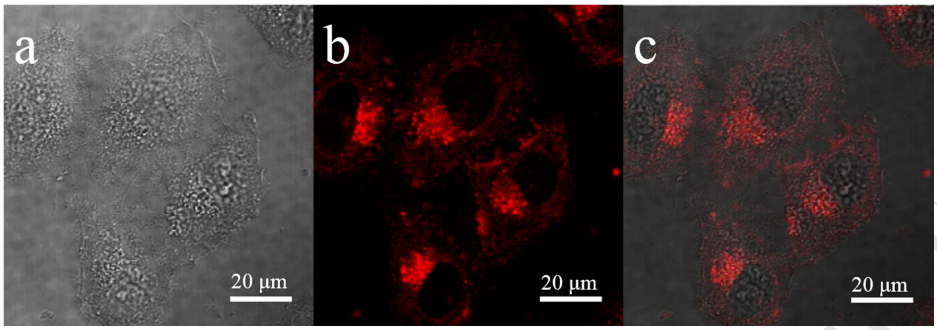

Figure 4

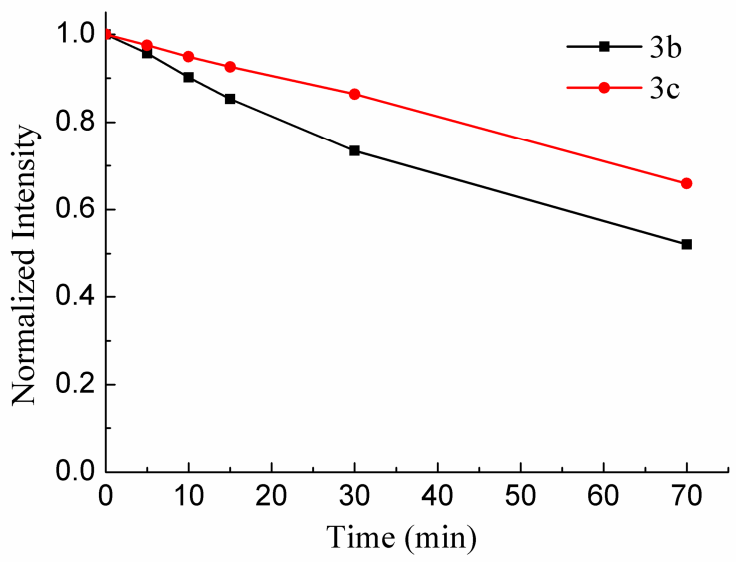

Figure 5

Highlights

Dicyanoboron Diketonate Dyes: Synthesis, Photophysical Properties and Bioimaging

- Dicyanoboron diketonates were synthesized and their optical properties were studied.
- The emission of the dyes was extended to the deep red region.
- The dyes exhibited high molar absorption coefficients and high photostability.

Supplementary data

Dicyanoboron Diketonate Dyes: Synthesis, Photophysical Properties and Bioimaging

Yan Zhou[a,b], Yu-Zhe Chen*[a], Jian-Hua Cao[a], Qing-Zheng Yang[a], Li-Zhu Wu[a], Chen-Ho Tung[a], Da-Yong Wu*[a]

[a] Technical Institute of Physics and Chemistry, Chinese Academy of Sciences, Beijing, 100190, China. Fax: +86 10 6255 4670; Tel: +86 10 8254 3772; E-mail: chenyuzhe@mail.ipc.ac.cn, dayongwu@mail.ipc.ac.cn

[b] University of The Chinese Academy of Sciences, Beijing, 100049, China

Contents:

1. Normalized excitation spectra of **3b** and **3c** in dichloromethane

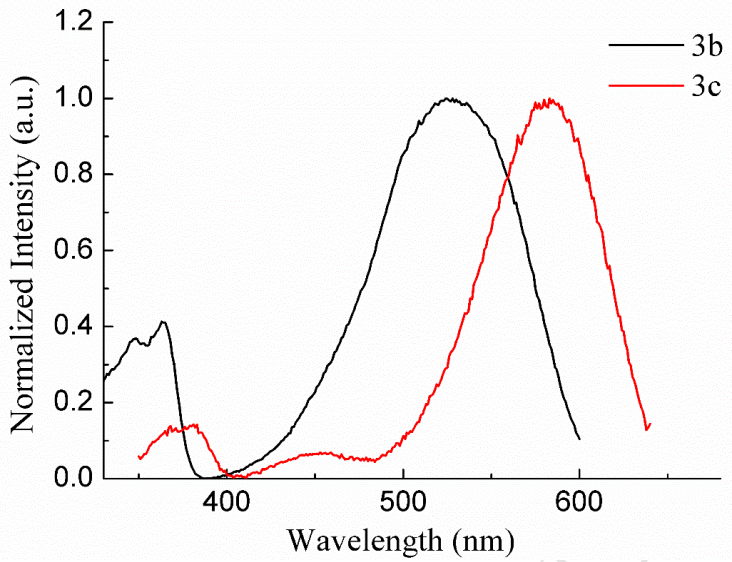

Figure S1. Normalized excitation spectra of **3b** and **3c** in dichloromethane: the emission wavelength of **3b** and **3c** were 619 nm and 657 nm, respectively.

2. Absorption spectra of **3b** and **3c** in various solvents

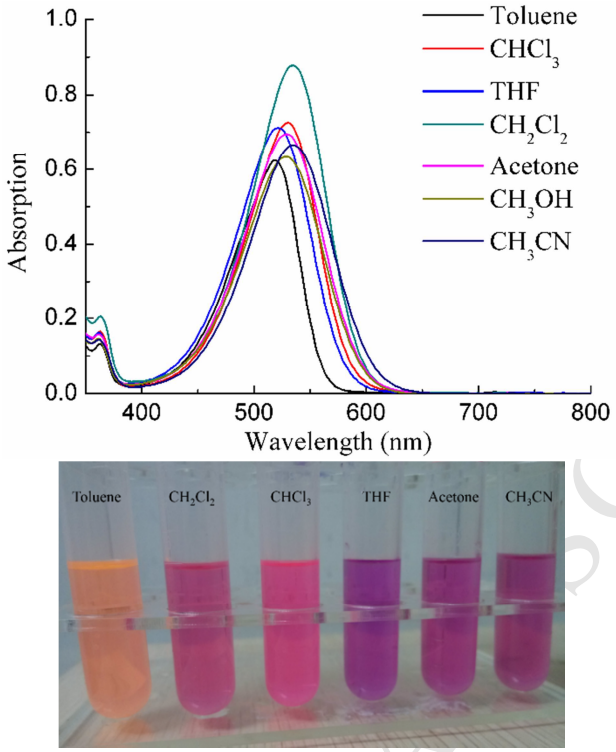

Figure S2. UV-vis absorption spectra and solution colors of **3b** in various solvents (1.0×10^{-5} M).

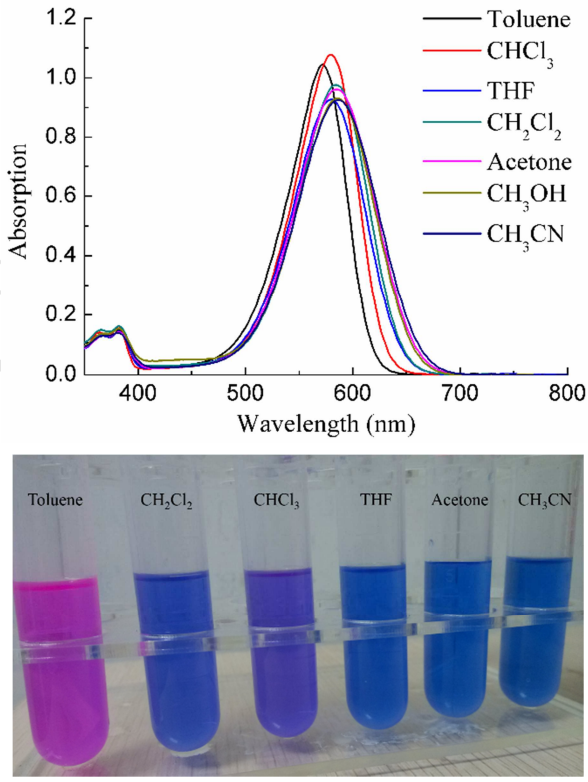

Figure S3. UV-vis absorption spectra and solution colors of **3c** in various solvents (1.0×10^{-5} M)

3. Cytotoxicity

HeLa Cells (5000 per well) were seeded in a 96-well plate and incubated overnight to allow cell attachment to the surface of the wells. After that, cells were replaced with fresh growth medium. **3c** solutions were added to obtain various final concentrations of 2, 4, 6, 8, 10 μM and incubated at 37 °C in a humidified atmosphere of 5% CO_2 for 4 h, then stained with CCK-8 (10 μL per 100 μL growth medium). The absorbance was measured at 450 nm using an EnSpire® Multimode Plate Reader (PerkinElmer, U.S.A.). The data represented the means of duplicate measurements in Figure S3.

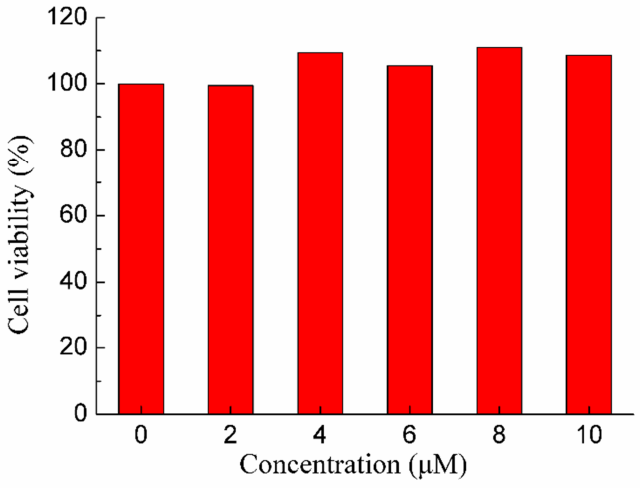

Figure S4**.** Cytotoxicity of **3c** in HeLa cells for 4 h incubation at 37 °C in a humidified atmosphere of 5% CO_2.

4. Synthetic route for **1a** and **2a**

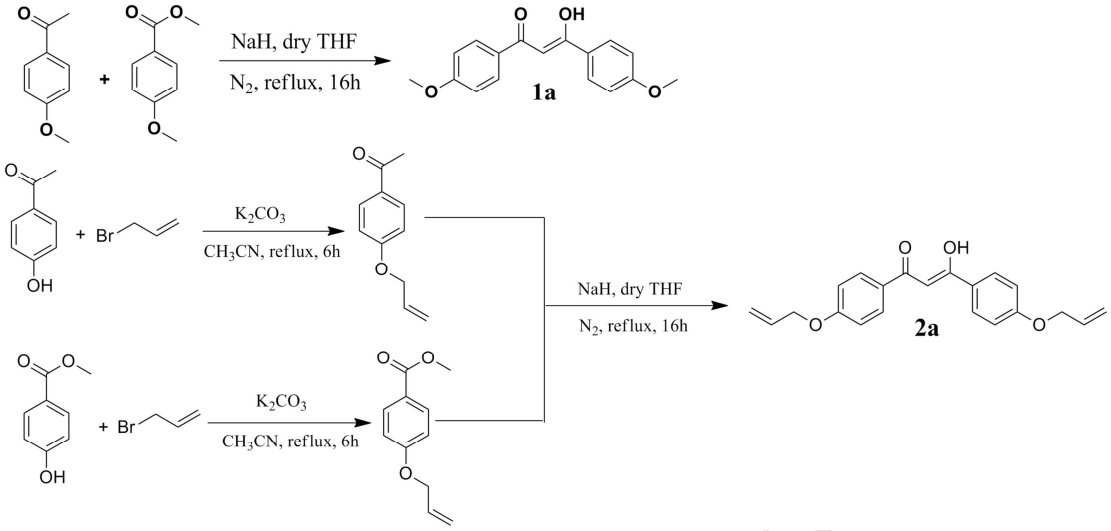

Scheme S1. The synthetic route for **1a** and **2a**.

4-allyloxy acetophenone was given as colorless liquid. Yield 99%. ^{1}H NMR (400 MHz, $CDCl_3$) δ 7.95 (d, J = 8.9 Hz, 2H), 6.96 (d, J = 8.9 Hz, 2H), 6.07 (ddd, J = 22.5, 10.5, 5.3 Hz, 1H), 5.44 (dd, J = 17.3, 1.5 Hz, 1H), 5.34 (dd, J = 10.5, 1.4 Hz, 1H), 4.62 (d, J = 5.3 Hz, 2H, OCH_2), 2.57 (s, 3H, CH_3). Methyl 4-allyloxy benzoate was given as colorless liquid by the same method. Yield 99%. ^{1}H NMR (400 MHz, $CDCl_3$) δ 7.98 (d, J = 8.9 Hz, 2H), 6.93 (d, J = 8.9 Hz, 2H), 6.05 (ddd, J = 22.5, 10.5, 5.3 Hz, 1H), 5.42 (dd, J = 17.3, 1.5 Hz, 1H), 5.31 (dd, J = 10.5, 1.3 Hz, 1H), 4.59 (d, J = 5.3 Hz, 2H, OCH_2), 3.88 (s, 3H, CH_3).

5. ^{1}H NMR and ^{13}C NMR spectra of **1a-3c**

^{1}H NMR of **1a** in $CDCl_3$

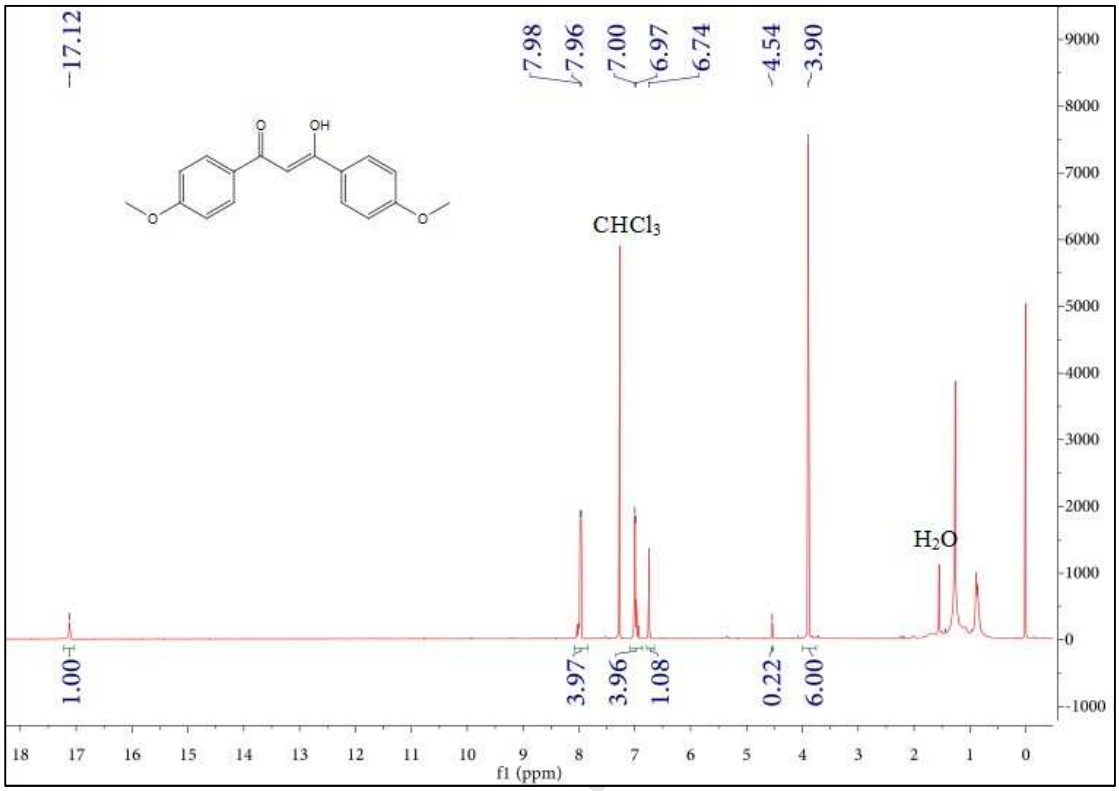

^{13}C NMR of **1a** in $CDCl_3$

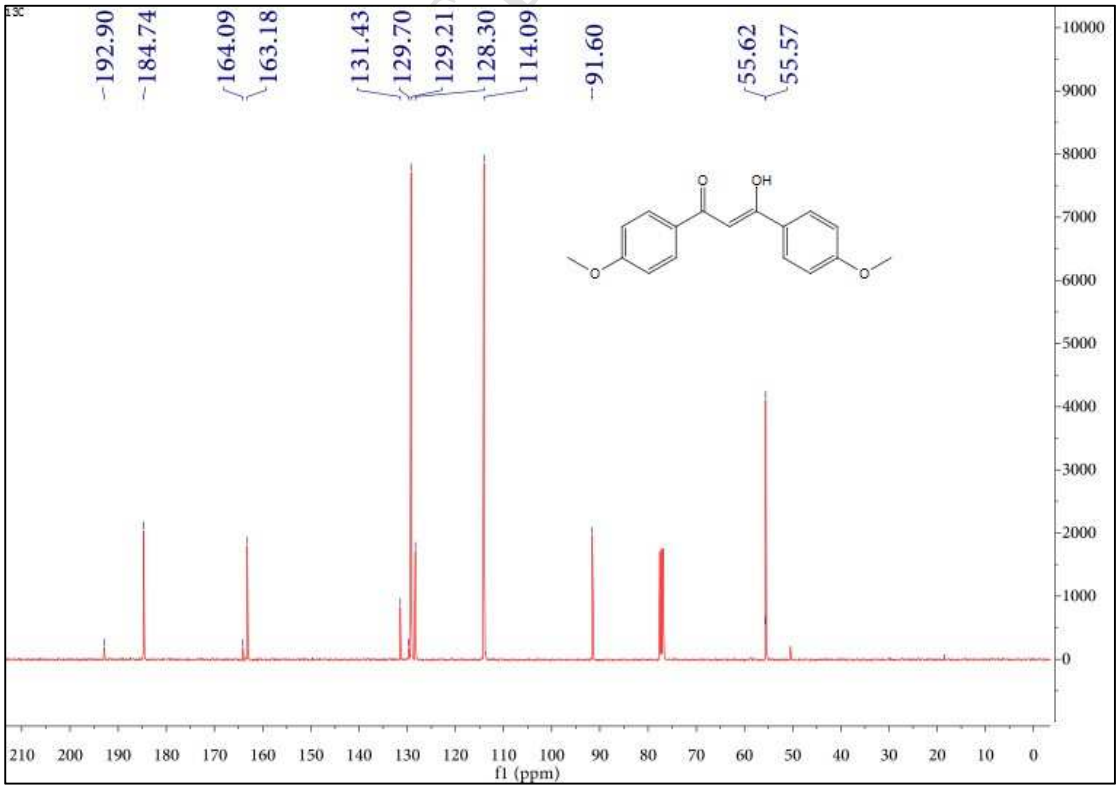

^{1}H NMR of **1b** in $CDCl_3$

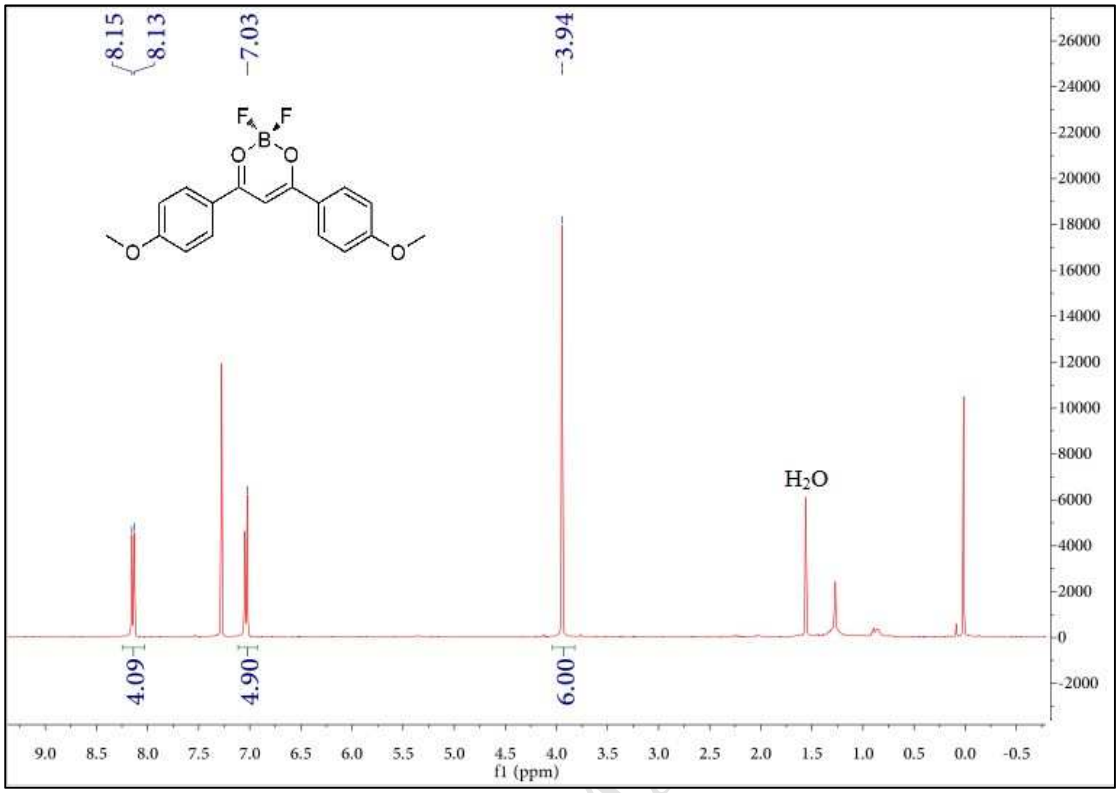

^{13}C NMR of **1b** in $CDCl_3$

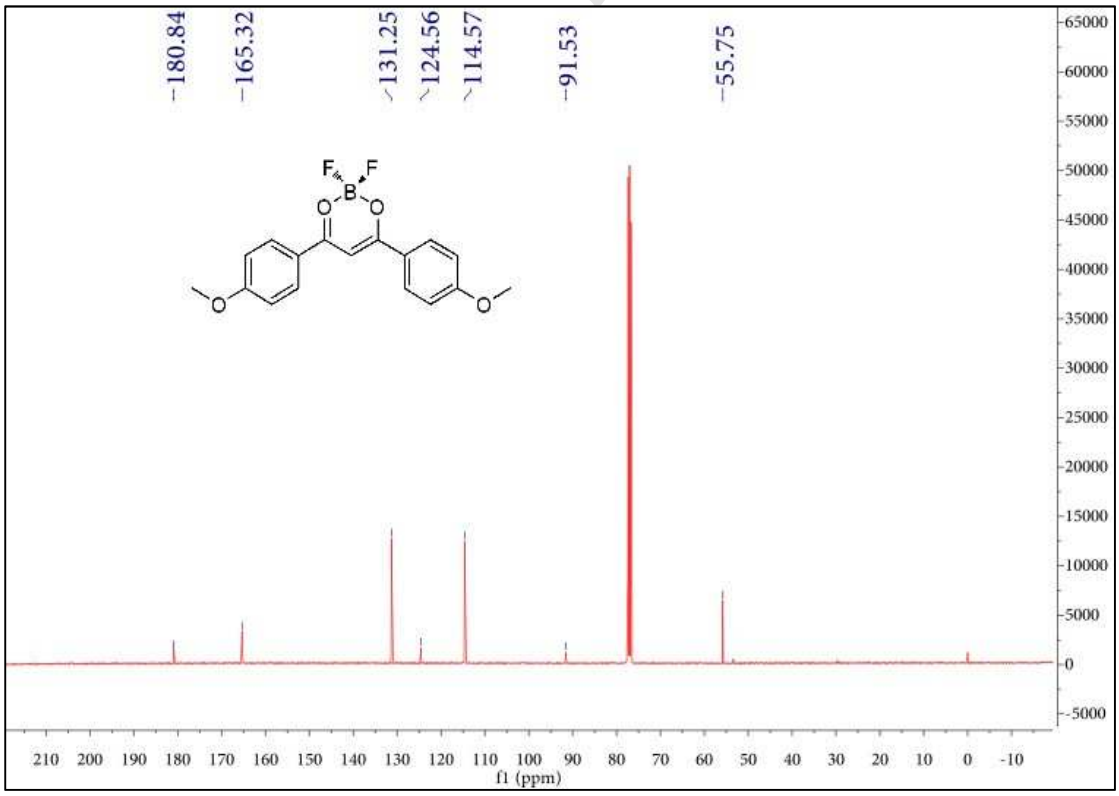

^{1}H NMR of **1c** in $CDCl_3$

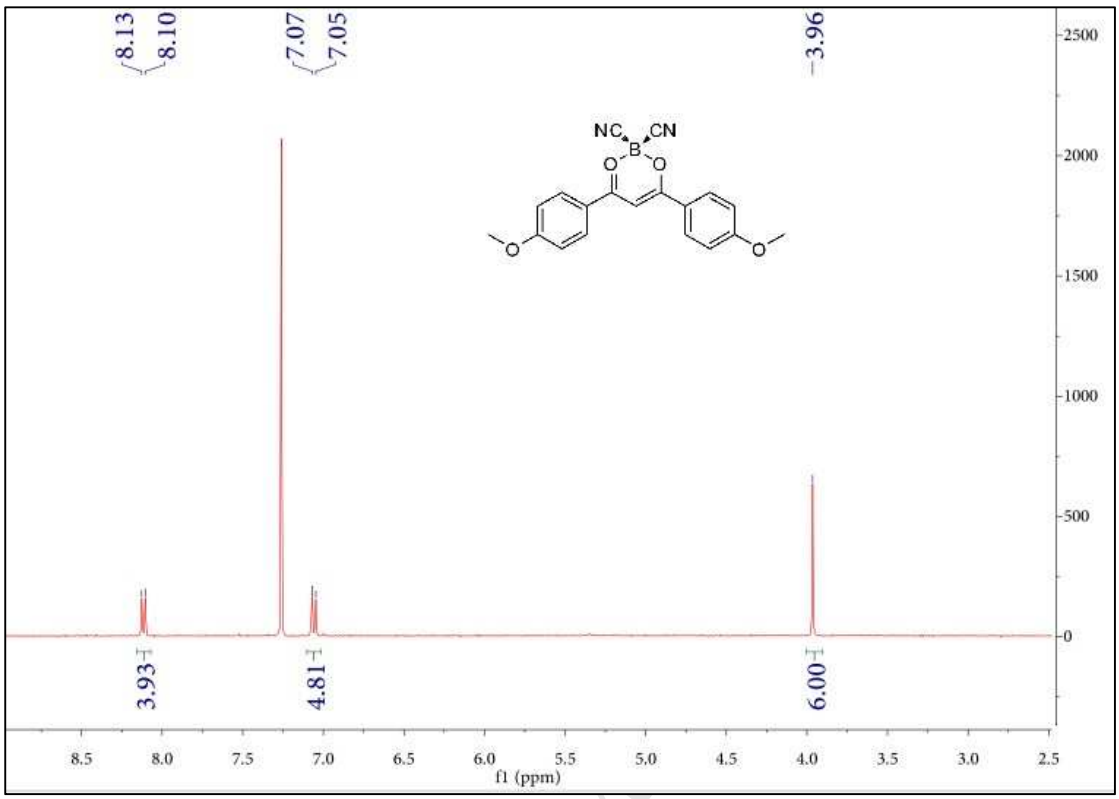

^{13}C NMR of **1c** in $CDCl_3$

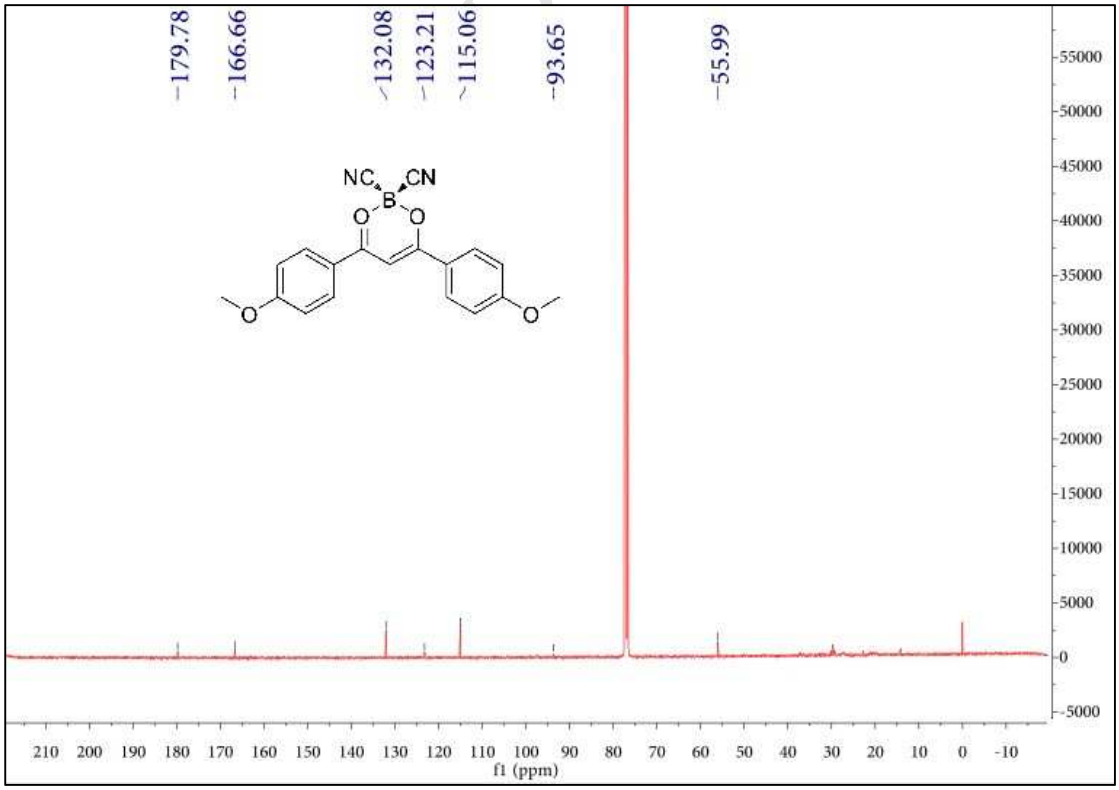

^{1}H NMR of **2a** in $CDCl_3$

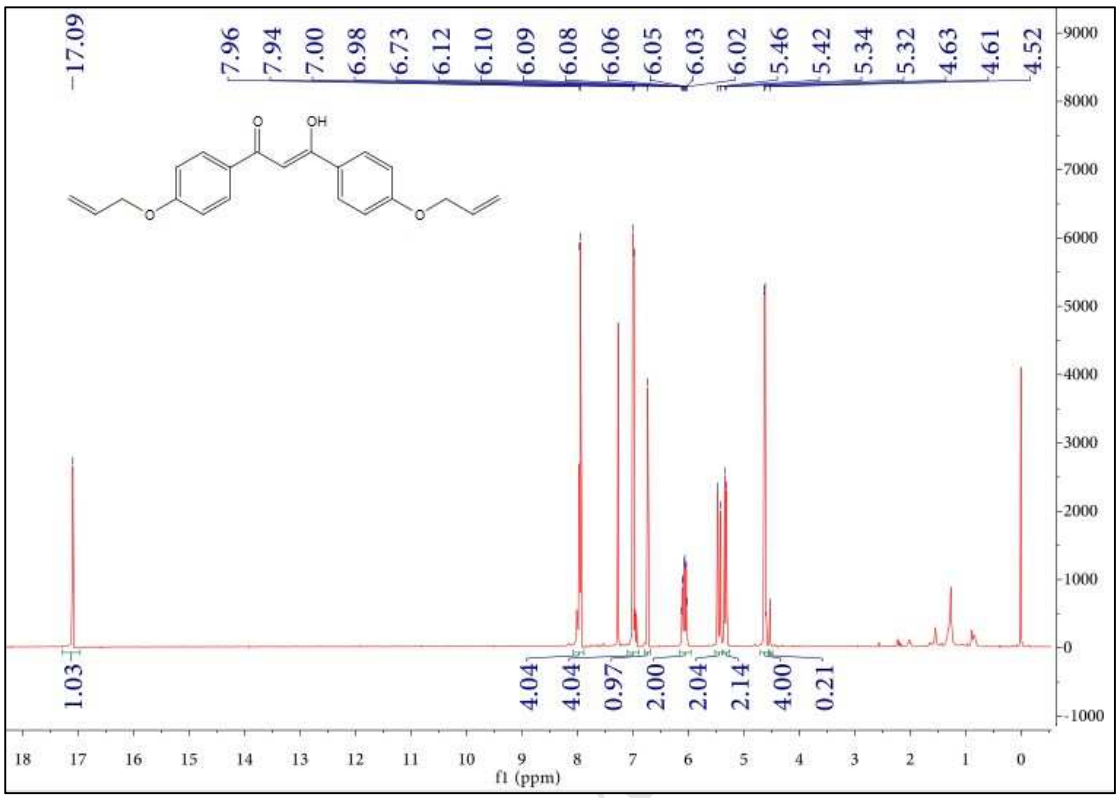

^{13}C NMR of **2a** in $CDCl_3$

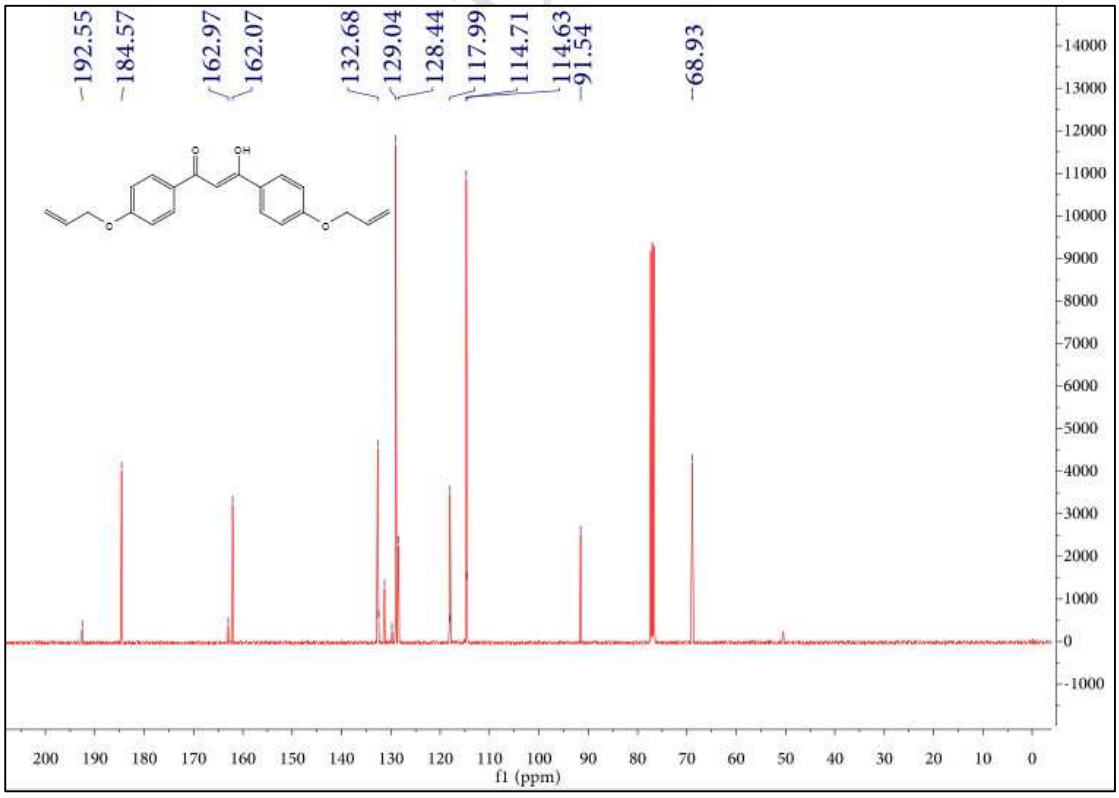

^{1}H NMR of **2b** in $CDCl_3$

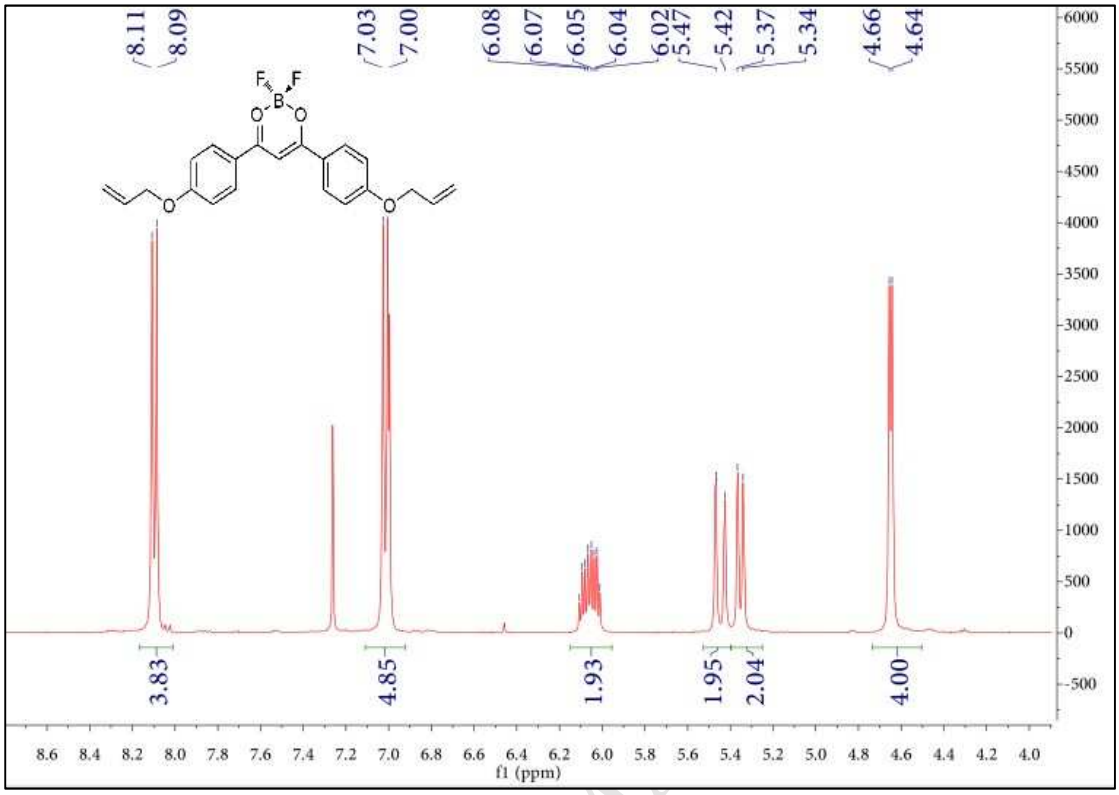

^{13}C NMR of **2b** in $CDCl_3$

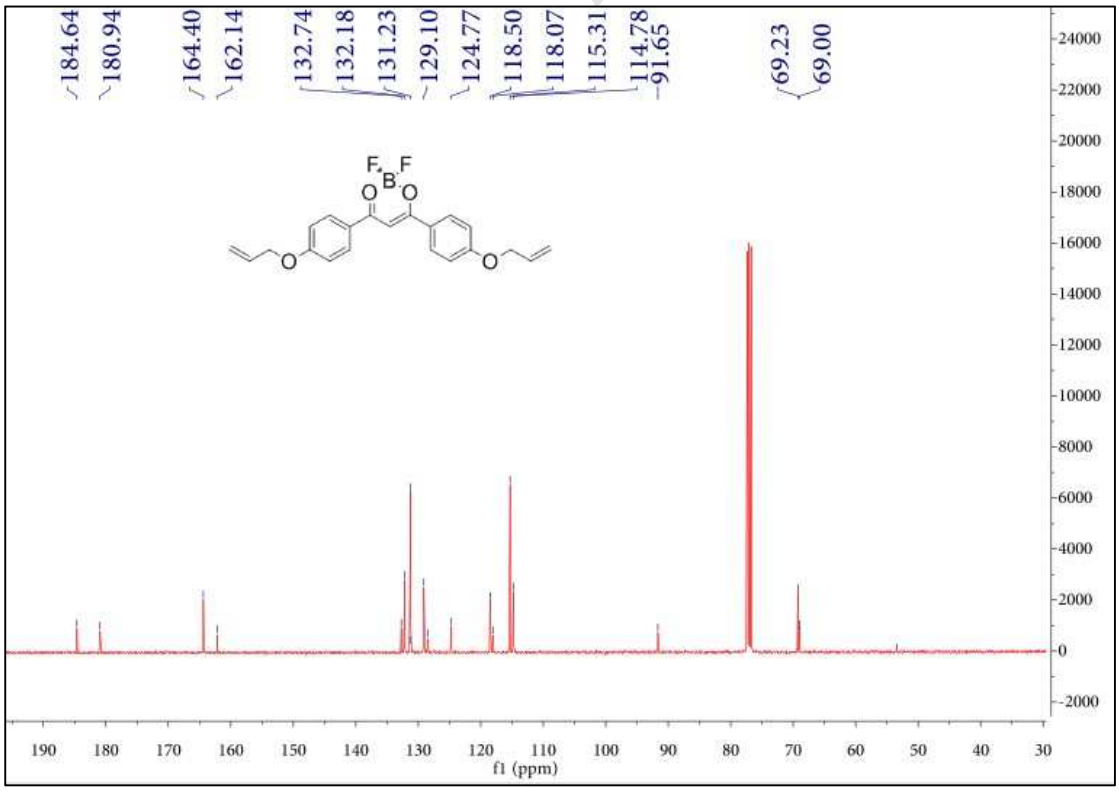

^{1}H NMR of **2c** in $CDCl_3$

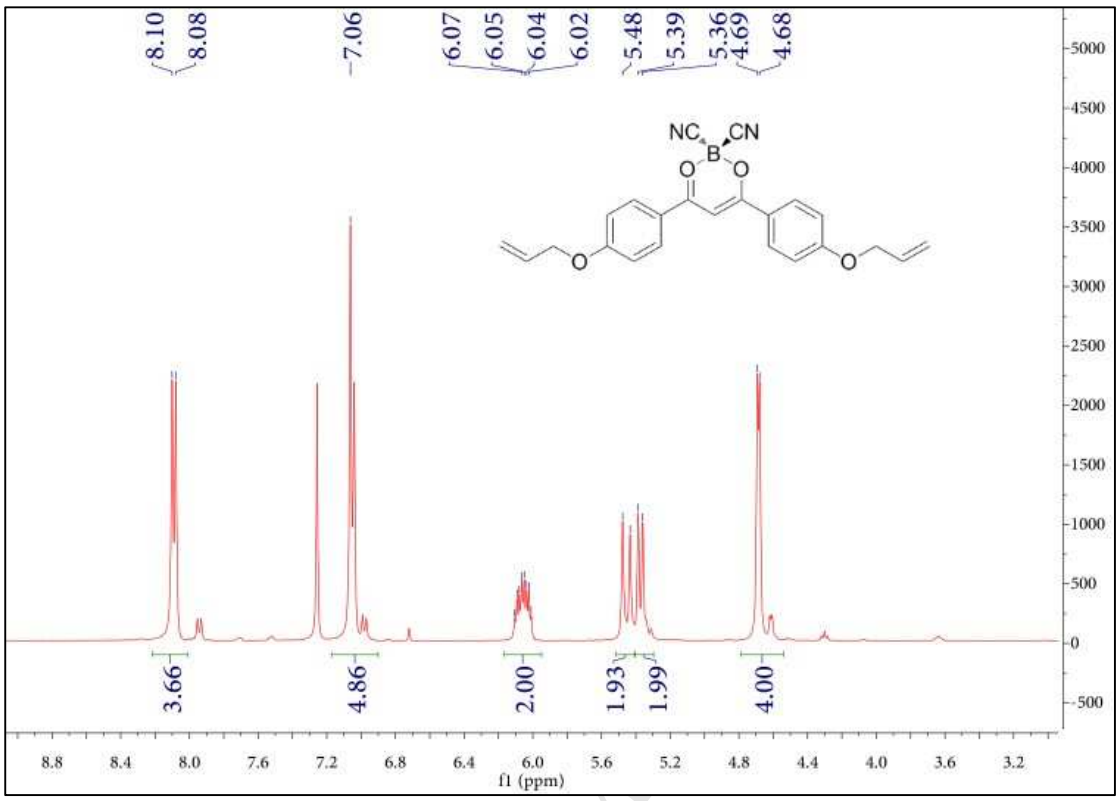

^{13}C NMR of **2c** in $CDCl_3$

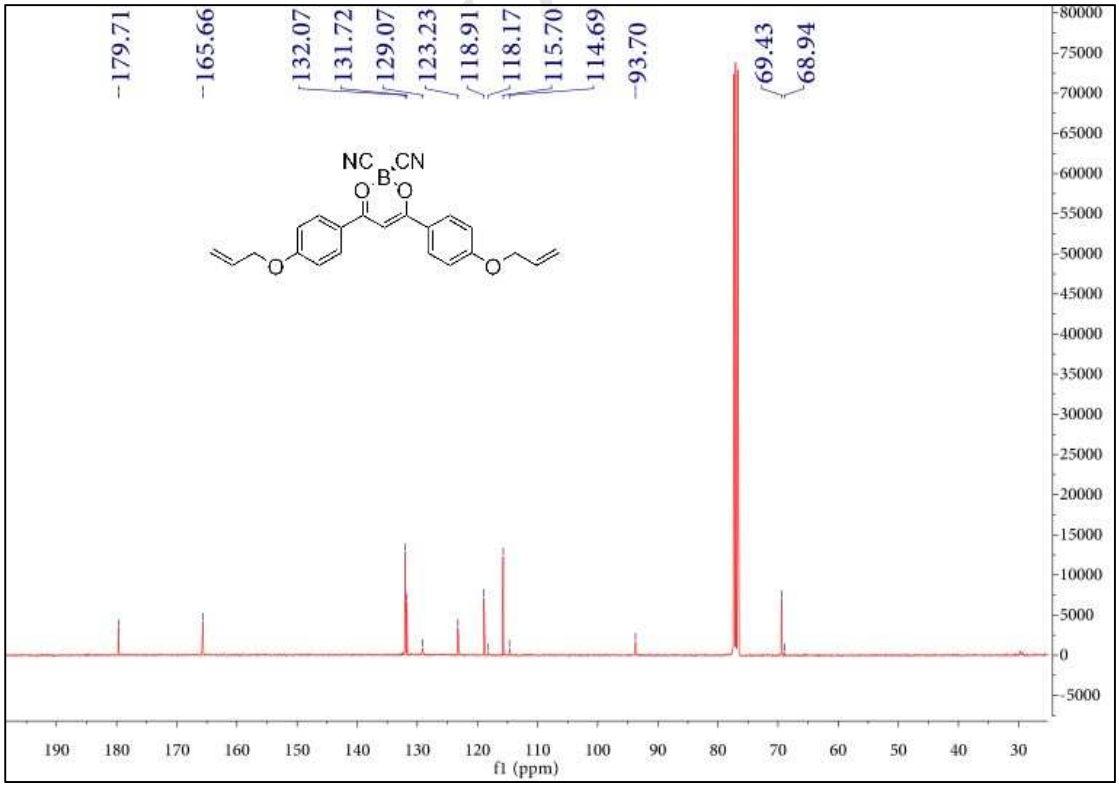

^{1}H NMR of **3a** in $CDCl_3$

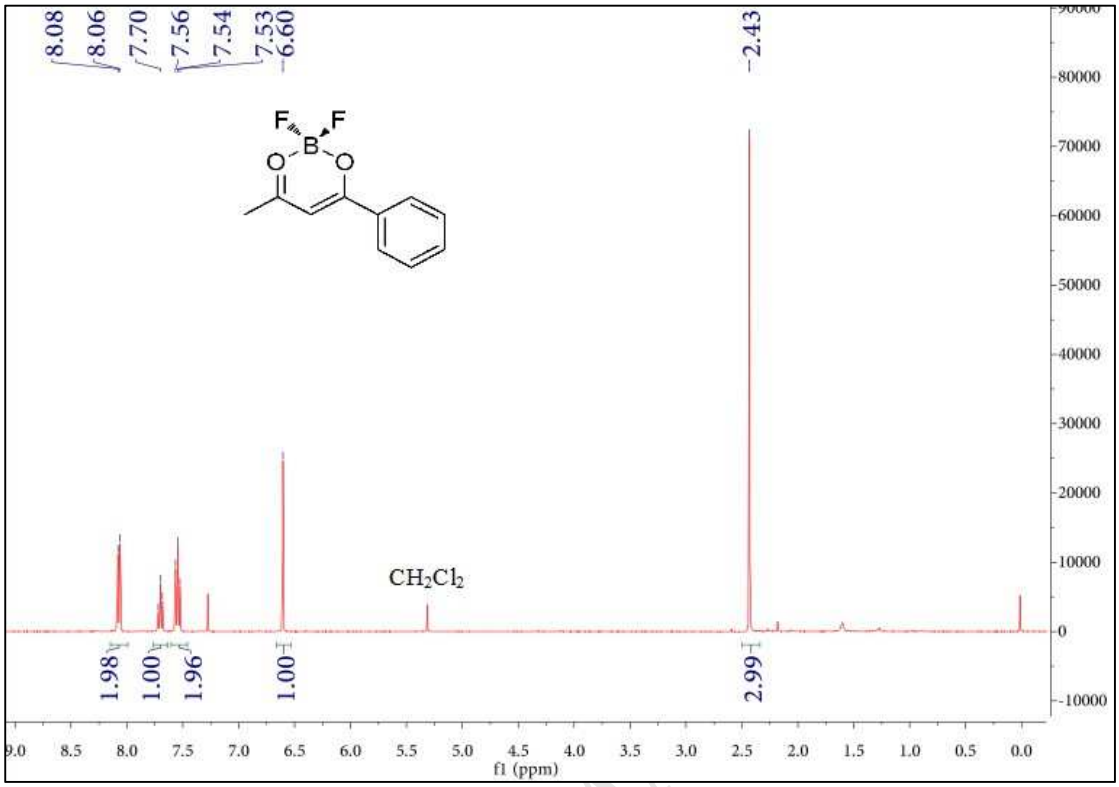

^{13}C NMR of **3a** in $CDCl_3$

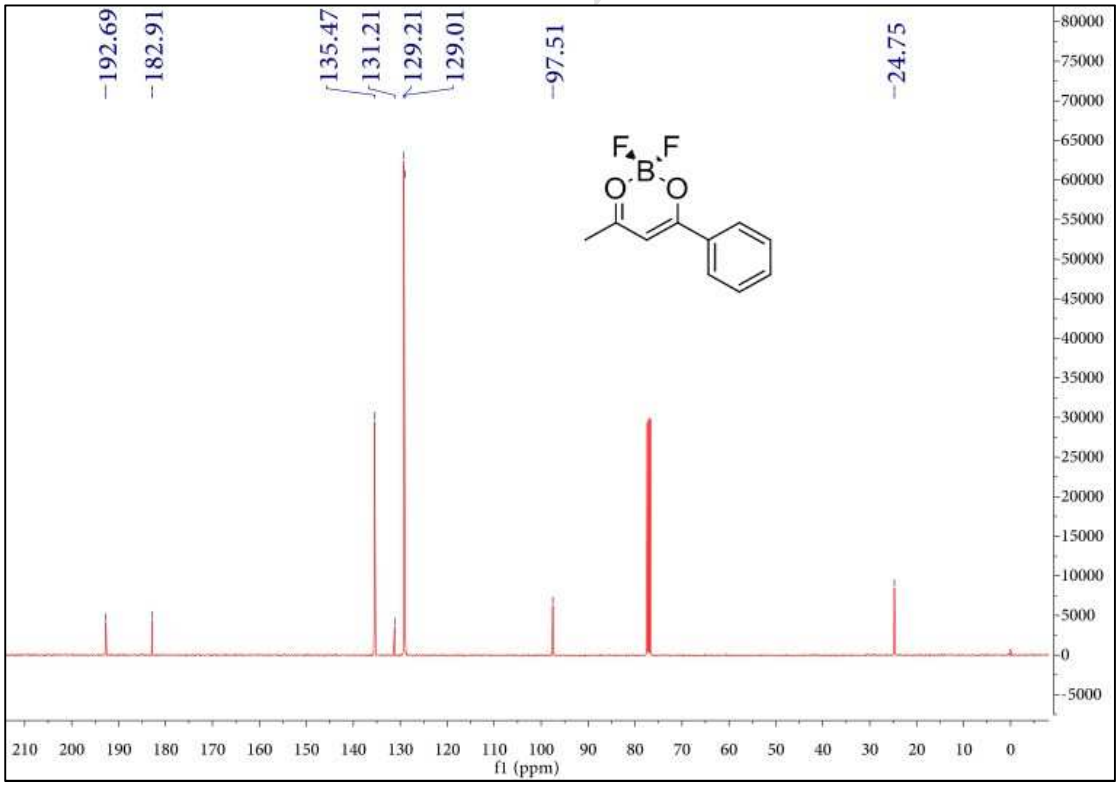

^{1}H NMR of **3b** in $CDCl_3$

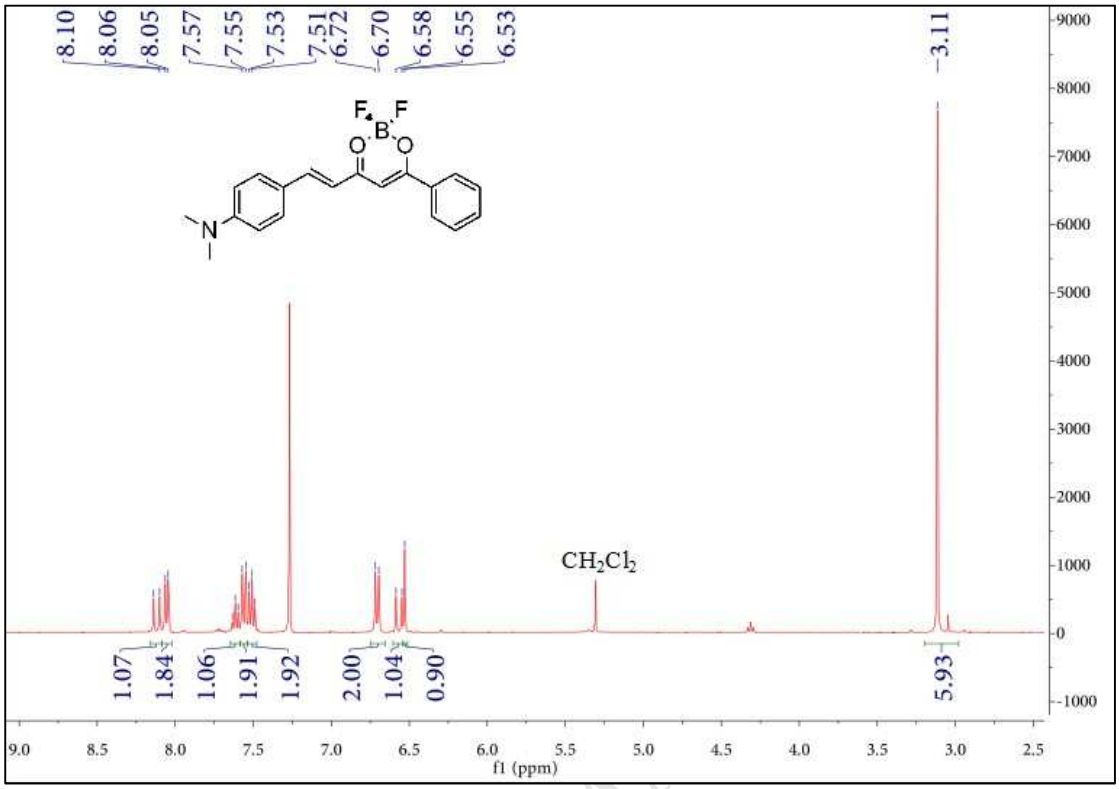

^{13}C NMR of **3b** in $CDCl_3$

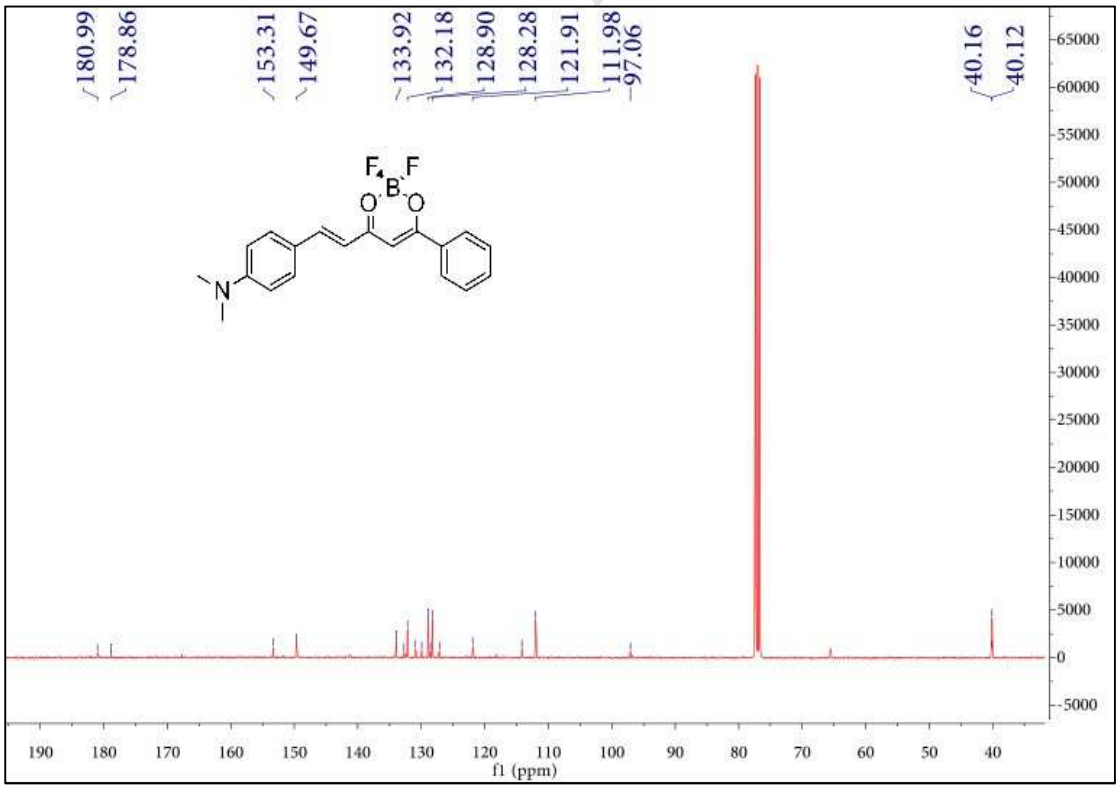

^{1}H NMR of **3c** in $CDCl_3$

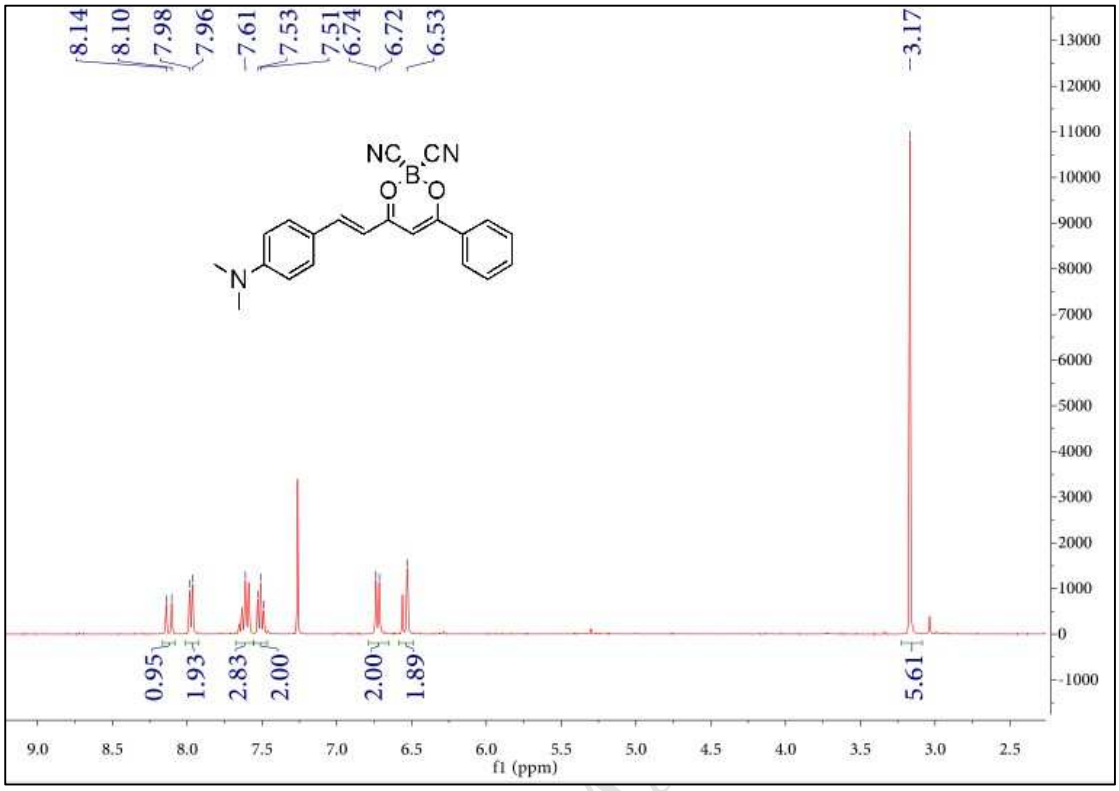

^{13}C NMR of **3c** in $CDCl_3$

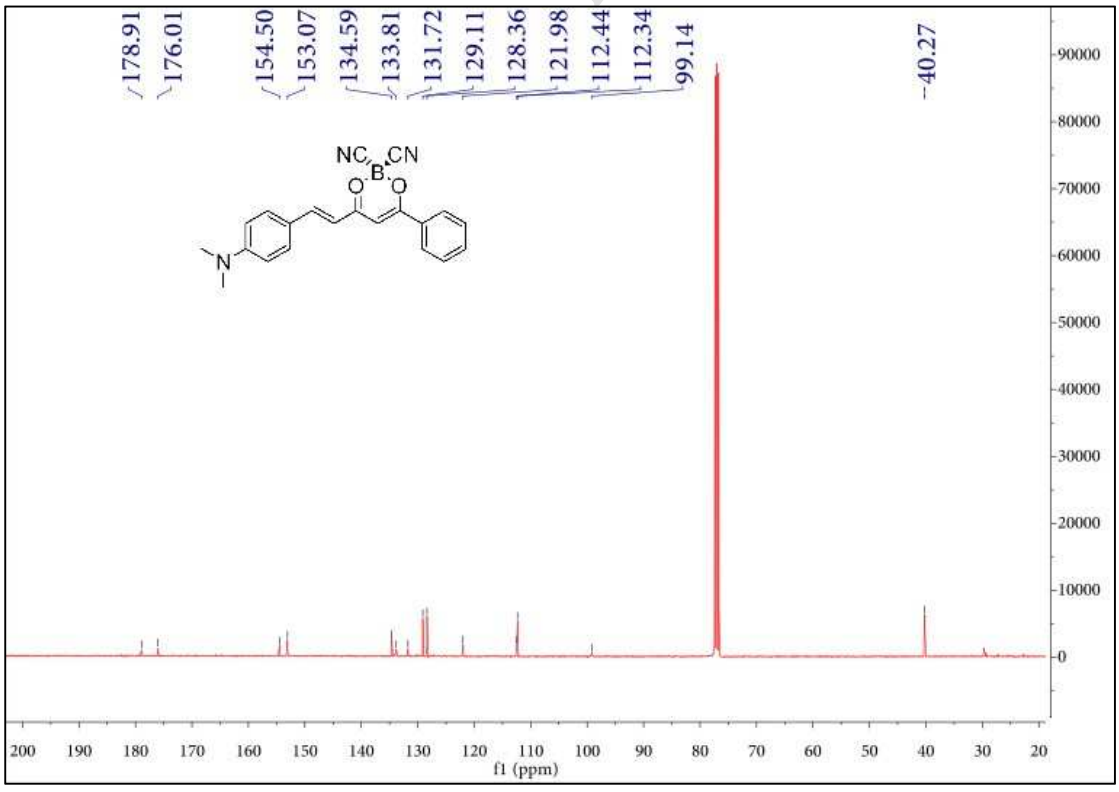

6. MS-EI of **1a**, **1b**, **2a**, **2b**, **3a**

MS-EI of **1a**

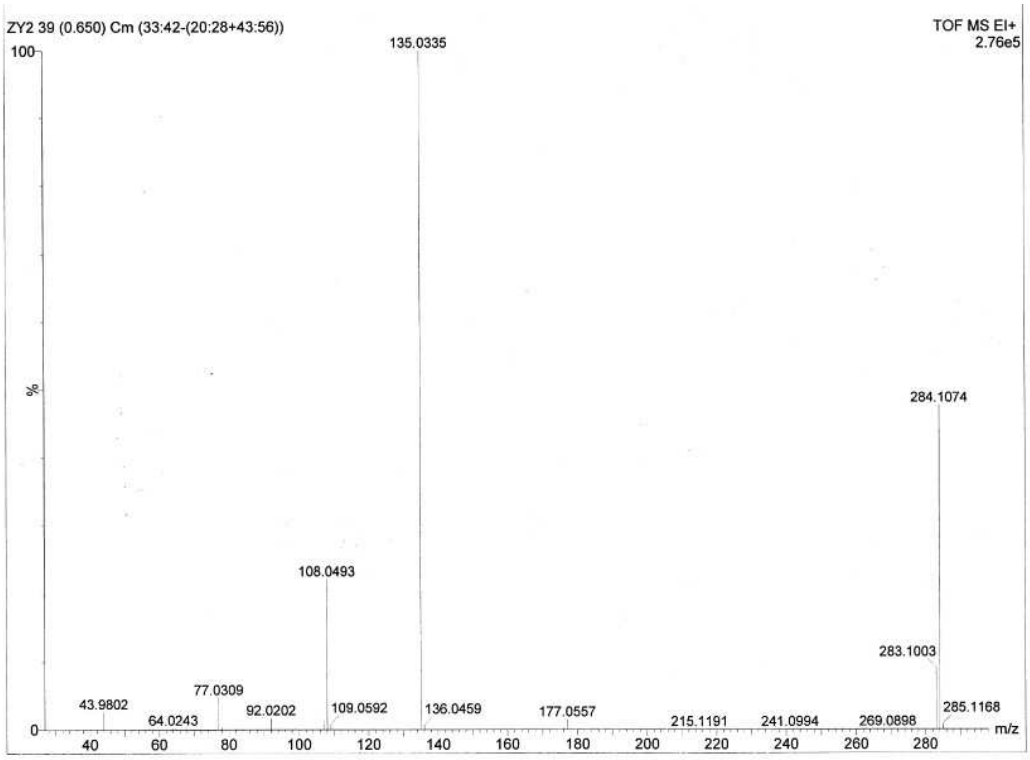

MS-EI of **1b**

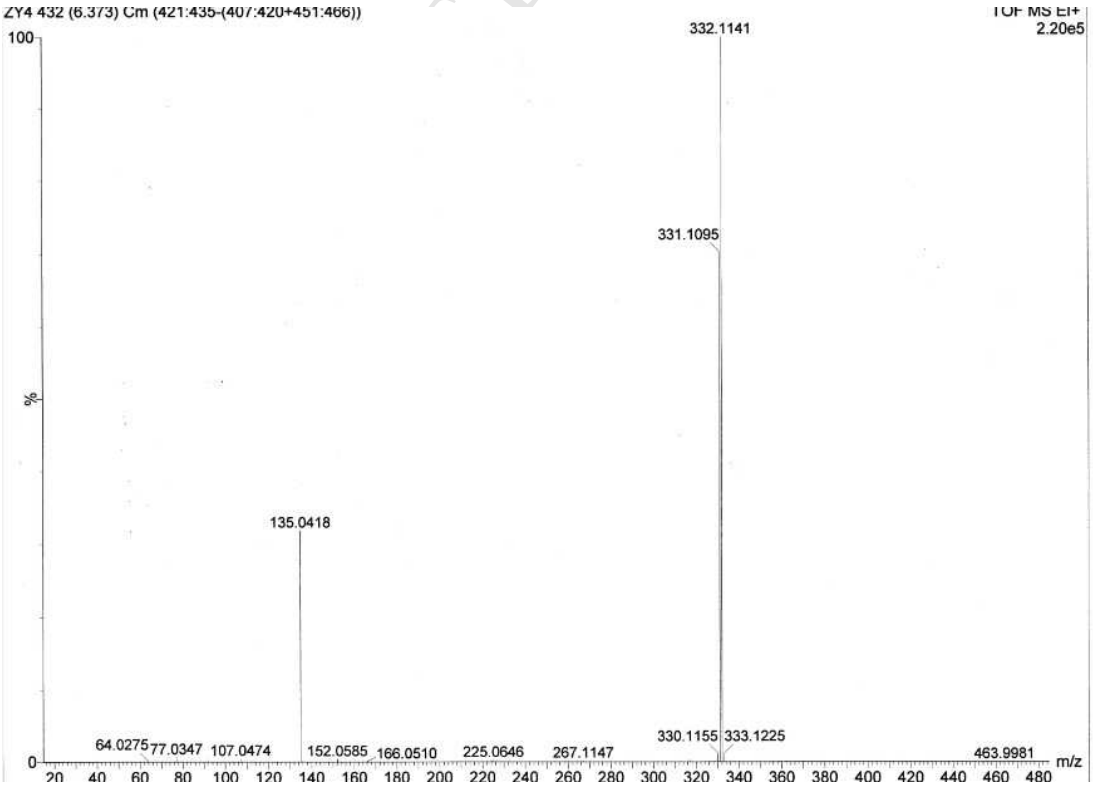

MS-EI of **2a**

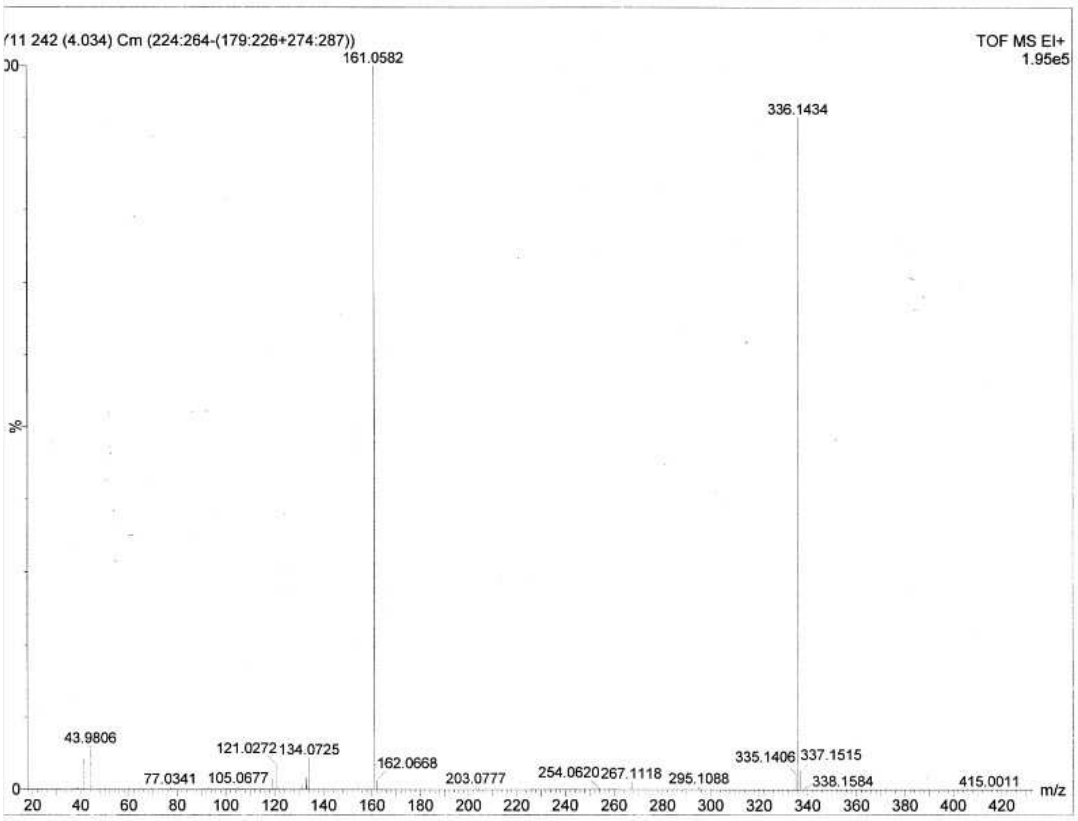

MS-EI of **2b**

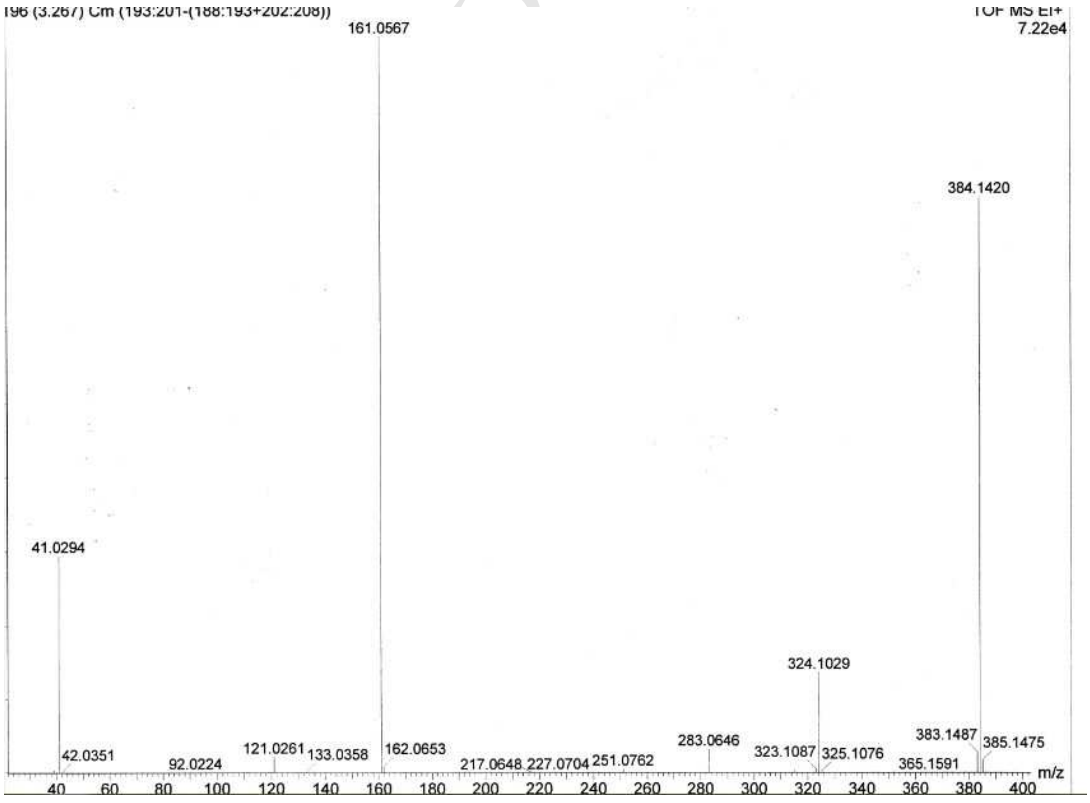

MS-EI of **3a**

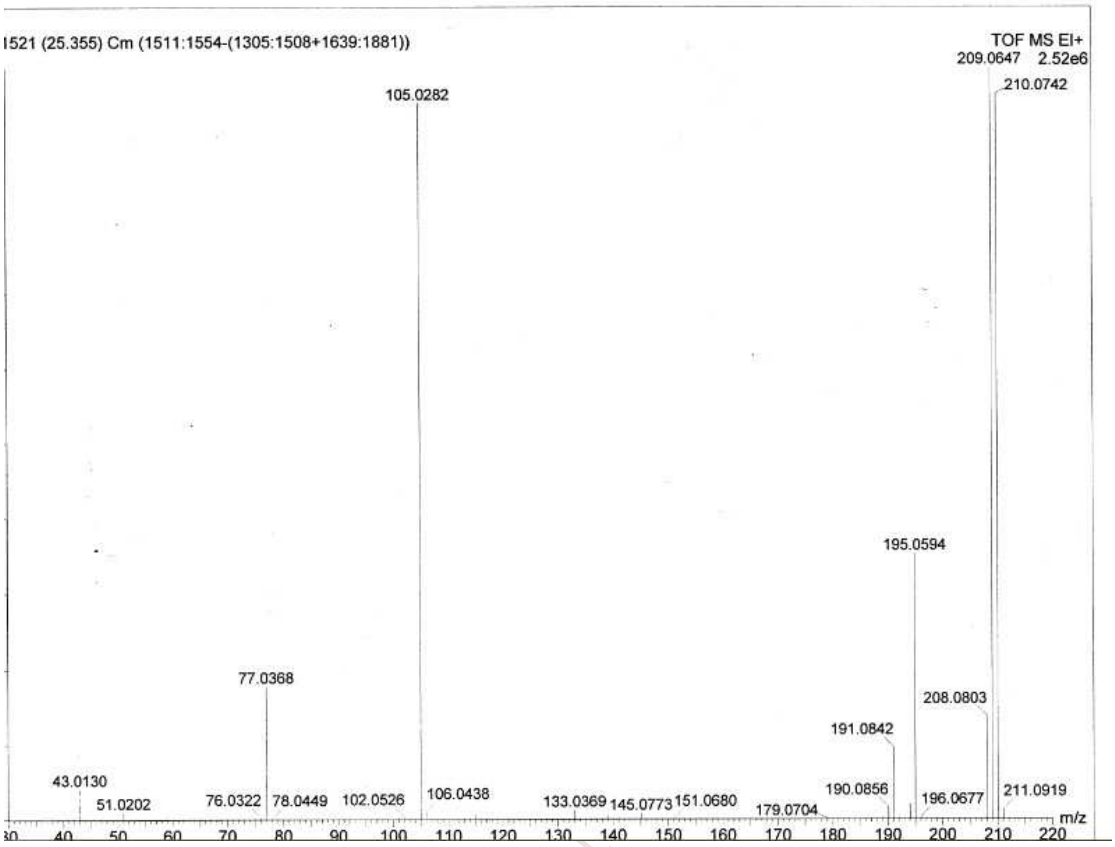

7. HRMS-ESI of **1c**, **2c**, **3b**, **3c**

HRMS-ESI of **1c**

Peking University Mass Spectrometry Sample Analysis Report

Analysis Info

Analysis Name	14030210_20140306_000001.d	Acquisition Date	3/6/2014 11:31:15 AM
Sample	1c	Instrument	Bruker Apex IV FTMS
Comment	ESI Positive	Operator	Peking University

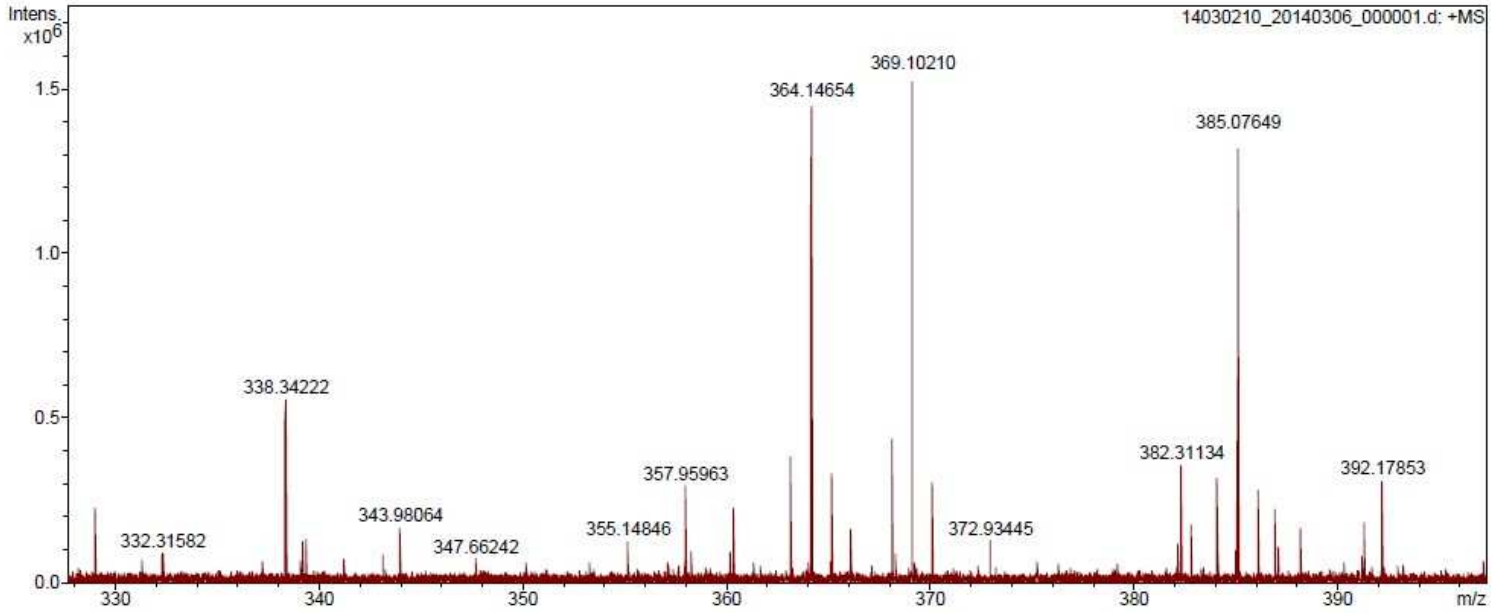

Meas. m/z	I	Formula	m/z	err [mDa]	err [ppm]	mSigma	rdb	e⁻ Conf	N-Rule
369.10210	1545369	C 19 H 15 B N 2 Na O 4	369.10205	-0.0	-0.1	28.8	13.5	even	ok

HRMS-ESI of **2c**

Peking University Mass Spectrometry Sample Analysis Report

Analysis Info

Analysis Name	14030210_20140306_000003.d	Acquisition Date	3/6/2014 11:36:54 AM
Sample	2c	Instrument	Bruker Apex IV FTMS
Comment	ESI Positive	Operator	Peking University

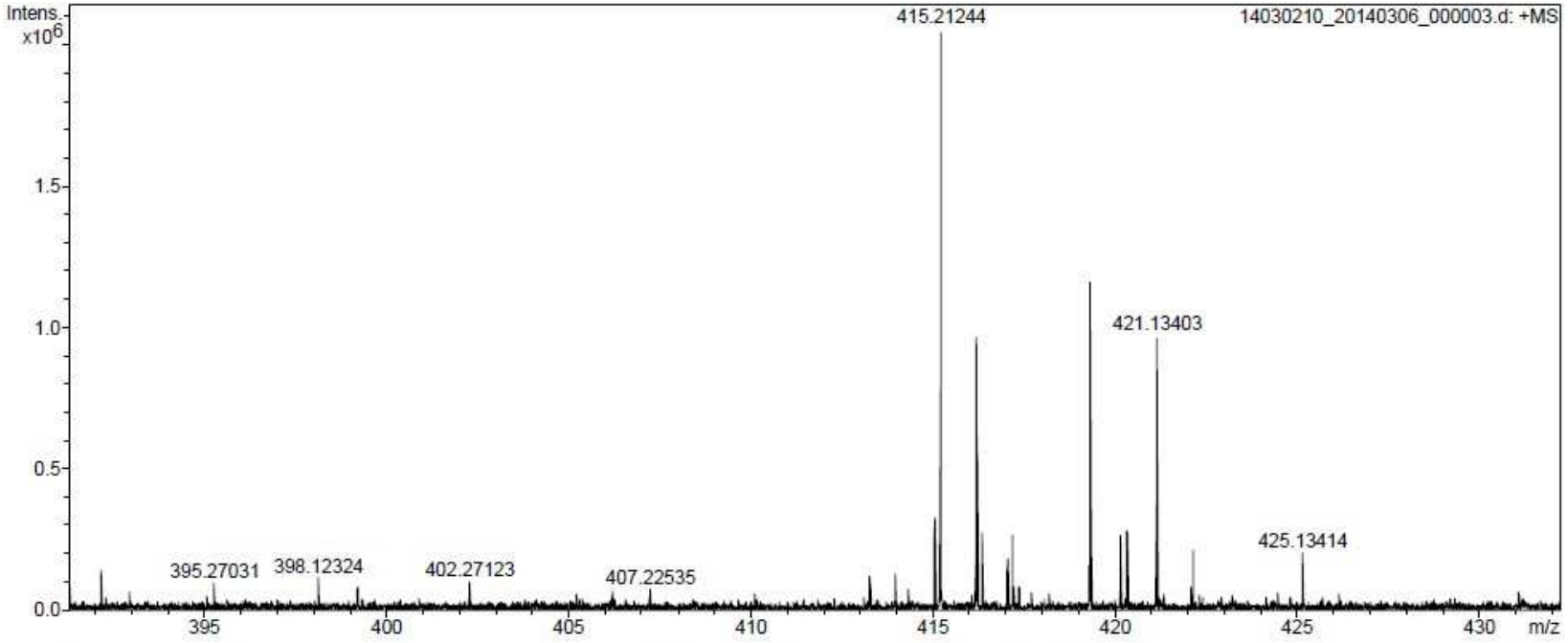

Meas. m/z	I	Formula	m/z	err [mDa]	err [ppm]	mSigma	rdb	e⁻ Conf	N-Rule
421.13403	976696	C 23 H 19 B N 2 Na O 4	421.13342	-0.6	-1.5	32.2	15.5	even	ok

HRMS-ESI of **3b**

Peking University Mass Spectrometry Sample Analysis Report

Analysis Info

Analysis Name	14030210_20140306_000004.d	Acquisition Date	3/6/2014 11:38:21 AM
Sample	3b	Instrument	Bruker Apex IV FTMS
Comment	ESI Positive	Operator	Peking University

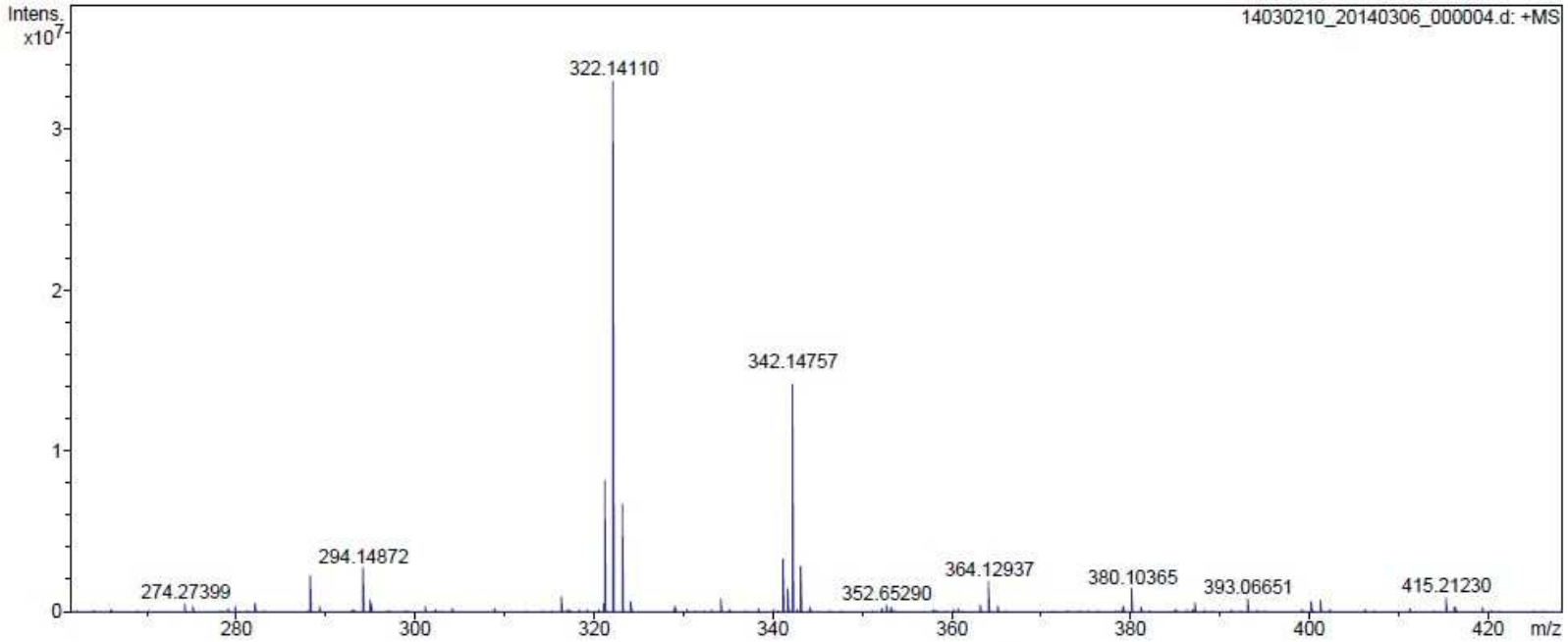

Meas. m/z	I	Formula	m/z	err [mDa]	err [ppm]	mSigma	rdb	e⁻ Conf	N-Rule
342.14757	14845302	C 19 H 19 B F 2 N O 2	342.14748	-0.1	-0.3	9.0	10.5	even	ok
364.12937	1946922	C 19 H 18 B F 2 N Na O 2	364.12943	0.1	0.2	12.5	10.5	even	ok

HRMS-ESI of **3c**

Peking University Mass Spectrometry Sample Analysis Report

Analysis Info

Analysis Name	13080335_20130822_000001.d	Acquisition Date	8/22/2013 2:13:25 PM
Sample	zy	Instrument	Bruker Apex IV FTMS
Comment	ESI Positive	Operator	Peking University

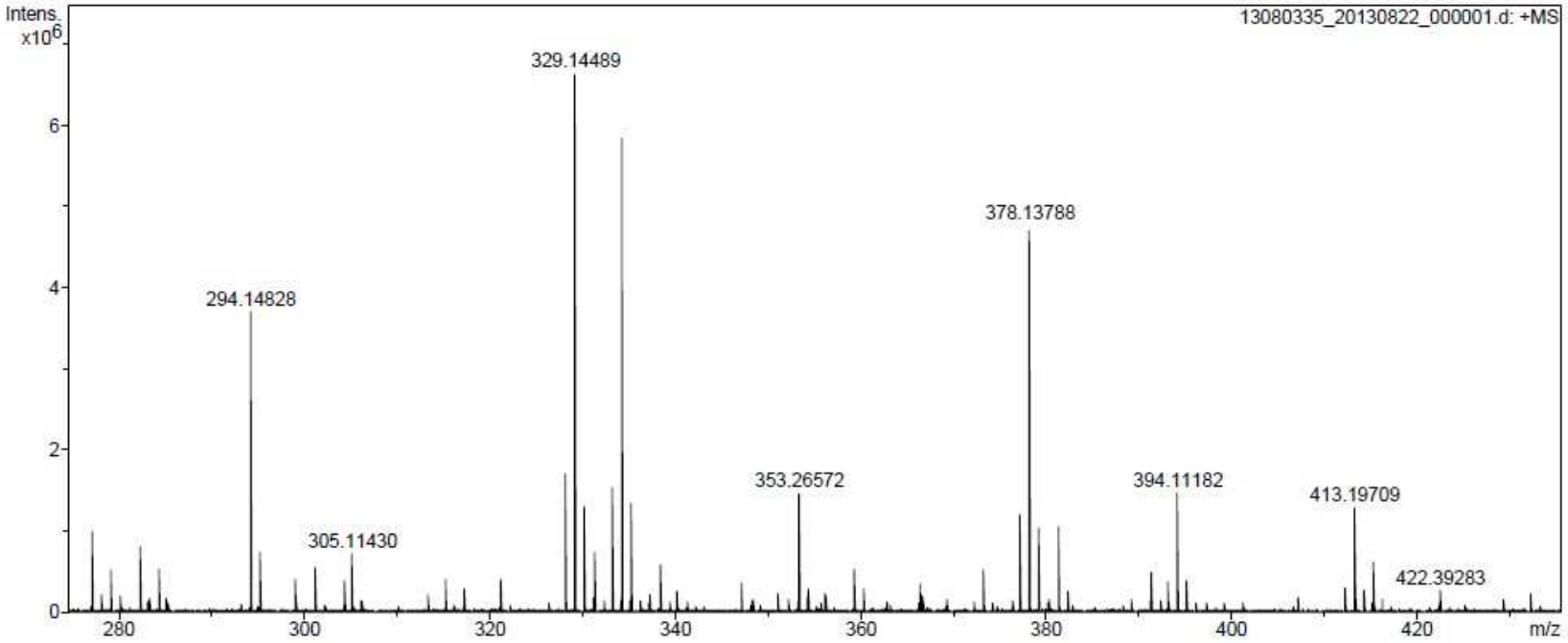

Meas. m/z	#	Formula	Score	m/z	err [mDa]	err [ppm]	mSigma	rdb	e⁻ Conf	N-Rule
378.13788	1	C 21 H 18 B N 3 Na O 2	100.00	378.13880	0.9	2.4	11.0	14.5	even	ok

8. FT-IR spectra of **1b**, **1c**, **2b**, **2c**, **3b**, **3c**

FT-IR spectra of **1b**

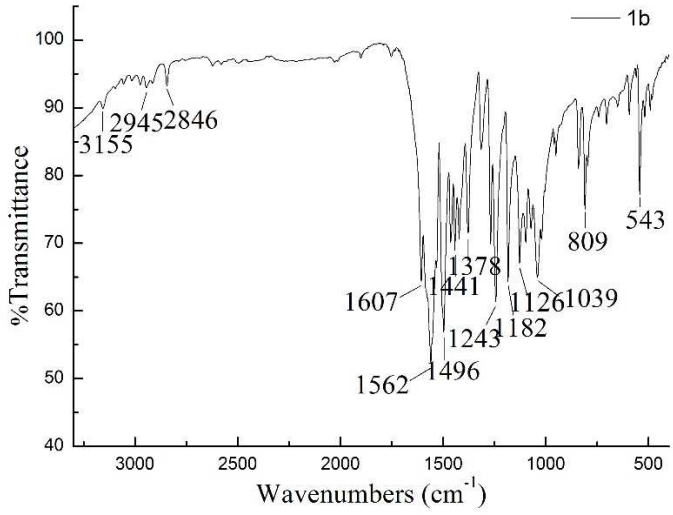

FT-IR spectra of **1c**

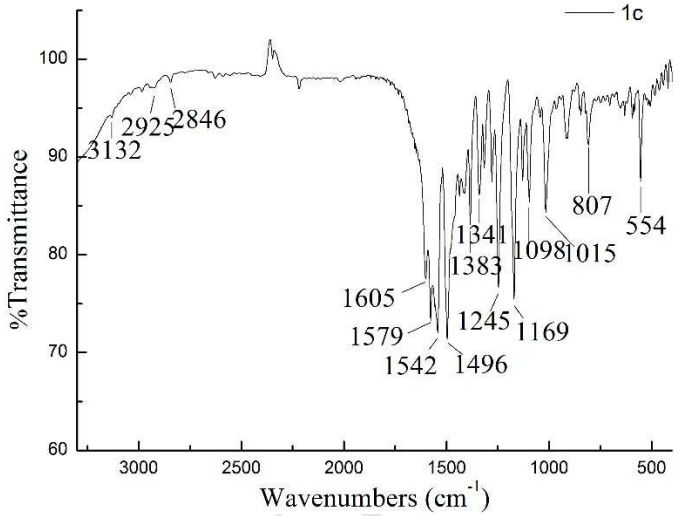

FT-IR spectra of **2b**

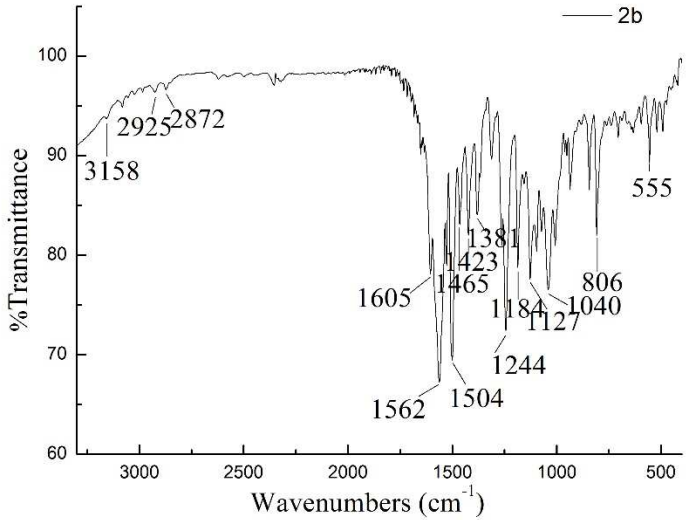

FT-IR spectra of **2c**

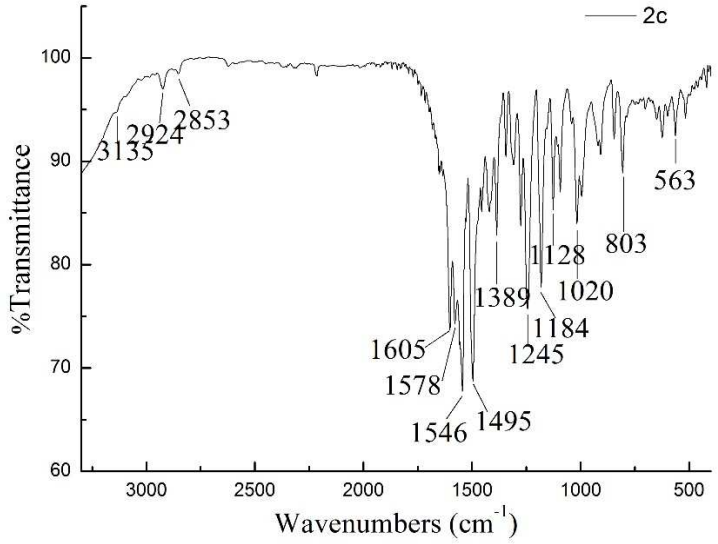

FT-IR spectra of **3b**

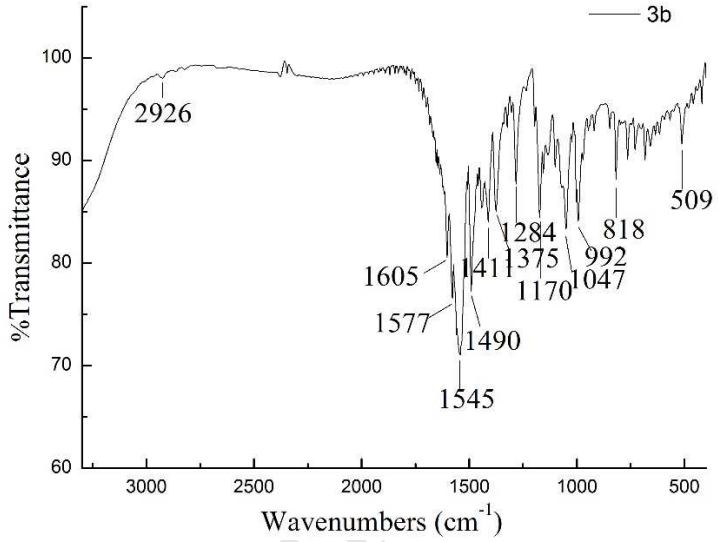

FT-IR spectra of **3c**